ESC European Society of Cardiology

Europace (2025) **27**, euaf083
https://doi.org/10.1093/europace/euaf083

TRANSLATIONAL RESEARCH

GSTP1 inhibits angiotensin II-induced atrial fibrillation by regulating ferroptosis

Han Li[1,2†], Zhenyu Feng[1†], Benke Li[3†], Jie Bai[4], Qiu-yue Lin[1], Xiaohong Yu[1], Ningning Zhang[1*], Yunpeng Xie[1*], and Xiaolei Yang[1*]

[1]Institute of Cardiovascular Diseases and department of Hematology, The First Affiliated Hospital of Dalian Medical University, Lianhe Road 193, Dalian 116000, People's Republic of China; [2]Department of Cardiology, Jinzhou District First People's Hospital Affiliated to Dalian University, Sidalin Road 683, Dalian 116000, People's Republic of China; [3]Department of Interventional Therapy, Dalian Sixth People's Hospital, Luganghuibai Road 269, Dalian 116000, People's Republic of China; and [4]Department of Occupational and Environmental Health, Dalian Medical University, No. 9 West Section Lvshun South Road, Dalian 116000, People's Republic of China

Received 19 December 2024; accepted after revision 31 March 2025; online publish-ahead-of-print 5 April 2025

Aims Atrial fibrillation is the most common arrhythmia in clinical practice and increases the potential risk of stroke, thromboembolism, and death. Glutathione-S-transferases pi 1 (GSTP1), a key factor of ferroptosis, can participate in stress signal and cell damage pathway through its non-catalytic activity, and has the role of regulating and protecting cells from carcinogens and electrophilic compounds. However, the role and mechanism of GSTP1 in angiotensin II-induced atrial fibrillation have not been studied.

Methods and results We constructed a mouse model of atrial fibrillation using Ang II and identified key factors by proteome and ferroptosis PCR array. We investigated the role of GSTP1 in atrial remodelling and NRAMs by the ferroptosis inhibitor Ferrostatin-1 (Fer-1), AAV9-cTNT-GSTP1, and GSTP1 inhibitor Ezatiostat. The results showed that the ferroptosis pathway was significantly altered in atrial fibrillation by proteomics. The ferroptosis inhibitor Fer-1 demonstrated that inhibiting ferroptosis can intervene in Ang II-induced atrial fibrillation. The ferroptosis PCR array showed that the expression of GSTP1 was significantly decreased in atrial fibrillation, and it was verified in cells and human atrial tissues. In mice infected with AAV9-cTNT-GSTP1, it was found that overexpression of GSTP1 inhibited Ang II-induced atrial fibrillation. Overexpression of GSTP1 inhibited Ang II-induced myocardial injury, oxidative stress, and ferroptosis *in vitro*.

Conclusion Therefore, these results preliminarily demonstrate that GSTP1-mediated ferroptosis plays a crucial role in the Ang II-induced atrial fibrillation model and can be considered a potential therapeutic target for atrial fibrillation.

* Corresponding author. Tel: +8618098870527; fax: +8641183635963. *E-mail address*: Zhangningning@dmu.edu.cn (N.Z.); Tel: +8618098873517; fax: +8641183635963. *E-mail address*: xieyunpeng@dmu.edu.cn (Y.X.); Tel: +8618098875725; fax: +8641183635963. *E-mail address*: yangxl1012@yeah.net (Xiaol.Y.)
† The first three authors contributed equally to the study.

Graphical Abstract

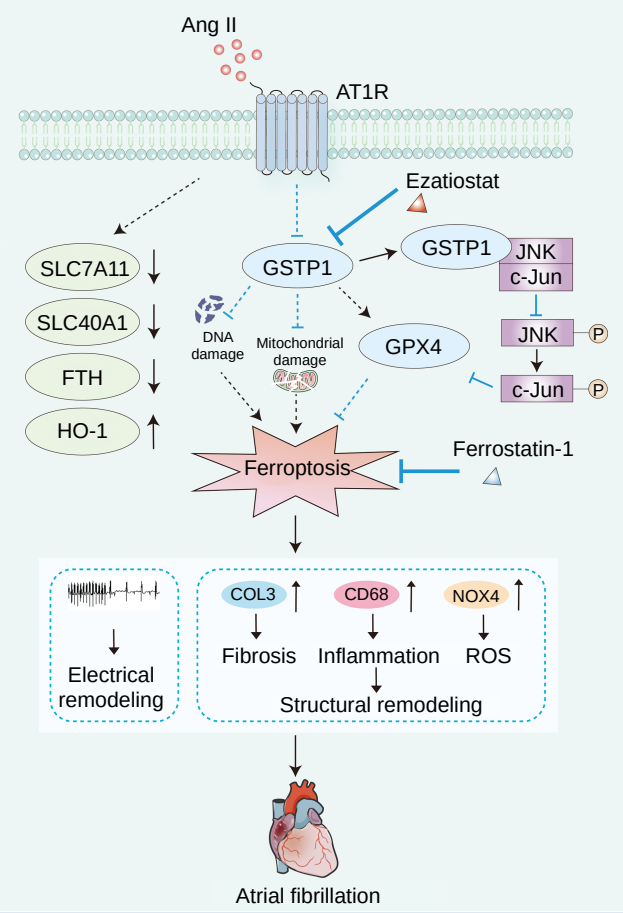

Keywords Ferroptosis • GSTP1 • Atrial fibrillation • Oxidative stress

What's new?

- Glutathione-S-transferases pi 1 (GSTP1) was significantly decreased in Ang II-induced mice atrial tissues and In the atrial tissue of patients with atrial fibrillation
- Overexpression of GSTP1 alleviates Ang II-induced atrial fibrillation by inhibits ferroptosis.
- Targeting GSTP1 may be an effective method to treat atrial fibrillation.

Introduction

As the most common form of persistent arrhythmia, atrial fibrillation (AF) has high morbidity and mortality, which brings great burden to medical and economic development.[1] The main pathological feature of AF is atrial structural remodelling, including enlarged compartments and fibrosis of parietal tissue. Angiotensin II (Ang II) is an important bioactive substance in the renin–angiotensin system, which plays an important role in regulating inflammatory response, oxidative stress, atrial fibrosis, and ion channel abnormalities, and can increase AF susceptibility.[2,3]

Ferroptosis, as an iron-dependent non-apoptotic form of cell death, is mainly characterized by lipid peroxidation and iron overload.[4] In addition, the nuclear factor erythroid-2 related factor 2 (NRF2) with redox effects can regulate its downstream targeting factors to inhibit lipid peroxidation and ferroptosis, such as glutathione S-transferases P1 (GSTP1), ferritin heavy chain (FTH), glutathione peroxidase 4 (GPX4), haemoglobin oxygenase-1 (heme oxygenase-1, HO-1), the light chain of the cell membrane cystine/glutamate antitransporter (recombinant solution carrier family 7 member 11, SLC7A11), etc., ferroptosis pathway small molecule compounds (iron chelators, antioxidants, ferroptosis inhibitors) and genetic programming can alleviate or prevent cardiovascular diseases by inhibiting the ferroptosis pathway.[5,6]

The development of cardiovascular diseases is closely related to ferroptosis, which can promote ferroptosis through specific signalling pathways and metabolic pathways, thus promoting the occurrence of cardiovascular diseases.[7] Meanwhile, prospective cohort studies have shown that high intake of dietary heme iron is strongly associated with increased risk of heart disease and cardiovascular death.[8] Recent studies have also shown a potential association between ferroptosis and cardiac arrhythmias.[8] Overexpression of the antioxidant factor NRF2 attenuates atrial fibrillation-induced arrhythmia, inflammation, and cardiac fibrosis.[9] Furthermore, excessive alcohol consumption can trigger ferroptosis and increase susceptibility to atrial fibrillation.[10]

Glutathione S-transferase (GST) is an enzyme that catalyses glutathione binding.[11] Members of the GST enzyme superfamily belong to phase II detoxification enzymes, which can regulate the redox state

of cells through their antioxidant catalytic and non-catalytic effects.[12] GST is mainly divided into seven subtypes: alpha (α), sigma (σ), mu (μ), pi (π), theta (θ), omega (ω), and zeta, and GSTP1 is the most studied type in mammals with the ability to protect cells from carcinogens and cytotoxins.[13] GSTP1 is the most common isozyme in mammalian cells and can be involved in the regulation of stress signalling through its non-catalytic activity.[14] GSTP1 can be metabolized by catalysing the reaction of unsaturated acrolein with glutathione, thereby protecting cyclophosphamide-induced cardiotoxicity in mice.[15] GSTP1 prevents ionizing radiation (IR)-induced death of pancreatic cancer cells by inhibiting ferroptosis.[16] The mechanism of GSTP1 in atrial fibrillation is not completely understood. In this study, the mouse atrial fibrillation model was constructed by Ang II induction to study the mechanism of ferroptosis-related gene GSTP1 in atrial fibrillation.

Methods

Animals and treatment

C57BL/6J male mice (~22 g, 8 weeks old) were purchased from Liaoning Changsheng Biotechnology Co., Ltd. The mice were housed in a suitable environment with adequate food and water. All animal experiments were conducted according to the standards of the Dalian Medical University Animal Experiment Management Committee.

Establishment of atrial fibrillation model and treatment *in vivo*

An atrial fibrillation mouse model was established by subcutaneously implanting Alzet osmotic pumps infused with Angiotensin II (Ang II, 2000 ng/kg/min, Aladdin, Catalog No. A107852) for 21 days. The dosage of Ang II was calculated based on the weight of each mouse, and the mice were weighed 1 day before pump implantation to determine the required amounts of Ang II and acetic acid. The mice were anaesthetized with tribromoethanol (500 mg/kg, ip), and a 1 cm incision was made in the neck skin using ophthalmic scissors. The osmotic pump was implanted subcutaneously with the pump cap facing downward, and the wound was sutured.

To explore the supportive effect of ferroptosis on Ang II-induced mice, ferroptosis inhibitor, Ferrostatin-1 (Fer-1), was treated to Ang II mice. Mice were randomly divided into four groups: control group, Fer-1 group, Ang II group, and Ang II + Fer-1 group. In the Fer-1 group and Ang II + Fer-1 group, Fer-1 (1 mg/kg/day) was intraperitoneal injected 7 days prior to Ang II treatment.

Echocardiography

After 20 days of subcutaneous osmotic pump implantation in mice, the mice were anaesthetized by using isoflurane (1–2%), which can maintain stable physiological functions in animals, including heart rate, blood oxygen partial pressure, and blood pH levels. Their chest hair was removed, and ultrasound coupling agent was applied. The mice were then placed in a supine position on the operating table. During the procedure, the mouse's heart rate was maintained at ~450–500 beats per minute, and a 30 MHz ultrasound probe was used to locate the mouse's heart. Initially, the parasternal long-axis view was obtained to identify the heart's long-axis orientation. Subsequently, the apical four-chamber view was located, and the left atrial diameter (LAD) was measured from this view. Left atrial M-mode ultrasound data were recorded at the parasternal long-axis view. At least four consecutive beats were analysed and calculated using the included software. All measurements were performed in a blinded manner to ensure objectivity and reproducibility.

Electrical stimulation induces atrial fibrillation

Anaesthesia was induced in mice via intraperitoneal injection of tribromoethanol at 500 mg/kg (the most common anaesthetic, completely anaesthetized mice within 5 min and lasted ~10–40 min, suitable for experimental projects with long operation time). The mice were then fixed in position, and the skin on the right side of the neck was incised with ophthalmic scissors. The right jugular vein and its branches were bluntly dissected. A small incision was made in the external jugular vein to guide the Millar 1.1 F octapolar EP catheter into the right atrium and right ventricle. An automatic stimulator was used to deliver pulses starting from voltage amplitudes of 3.5, 5, and 8 V, in increasing order, with pacing cycle lengths decreasing from 40 to 20 ms (decreasing by 2 ms each time) to induce atrial fibrillation for 5 s. A computer data acquisition system (GY6328B; Henan Huanan Medical Science & Technology Ltd, Zhengzhou, China) recorded single-lead surface electrocardiograms and intracavitary bipolar electrograms. If a rapid irregular waveform persisted for more than 1 s after the 5 s pulse stimulation, it was considered that the mouse had atrial fibrillation. The occurrence and duration of atrial fibrillation in each mouse were recorded. End of experiment, the neck skin was bluntly dissected using tweezers to expose the right carotid artery. The right carotid artery was cut open with surgical scissors, and blood was collected into an EP tube using a syringe. After allowing the blood to stand for 10 min, the EP tubes were placed in a 4°C centrifuge at 3000 rpm for 15 min to separate the serum. The serum was then transferred into a new EP tube and stored at −80°C. The chest was opened to expose the heart. A 10 mL syringe filled with saline was inserted into the apex of the heart, and saline was injected until the liver tissue turned white, ensuring complete perfusion. The mice were euthanized by cervical dislocation while under anaesthesia. The heart was quickly excised using surgical scissors and placed in saline to remove excess blood. Excess blood vessels and fat tissue were carefully removed, and the heart was weighed. The ventricles were dissected away using a blade, and the remaining atrial tissue was processed further. A portion of the atrial tissue was fixed in an EP tube containing 4% paraformaldehyde for subsequent pathological sectioning. The remaining atrial tissue was placed directly into an EP tube, frozen at −80°C, and stored for later extraction of total RNA and protein. This procedure was performed immediately after the completion of the electrical stimulation experiments to ensure the integrity of the tissues for subsequent analyses.

Paraffin embedding

The atrial tissue was fixed in 4% paraformaldehyde at room temperature for 48 h. Subsequently, the atrial tissue was placed in a numbered embedding box for dehydration (85% ethanol → 95% ethanol → absolute ethanol I → absolute ethanol II → xylene I → xylene II). After soaking the tissue in liquid paraffin for 1 h, the atrial tissue was embedded in paraffin.

H&E staining

After de-waxing the heart tissue paraffin sections, the sections were immersed in haematoxylin staining solution (Solarbio, G1120) for 5 min, then rinsed with tap water for ~20 s. The sections were dipped in hydrochloric acid alcohol differentiation solution for 4 s, followed by a 10 min rinse in running water. The sections were then counterstained with eosin for 8 min, rapidly rinsed with tap water, dehydrated, and finally sealed with neutral resin.

Masson staining

The heart tissue paraffin sections were de-waxed, and then stained with Masson's trichrome staining (Solarbio, G1340). The tissue sections were soaked in Bouin's solution and stored overnight in the refrigerator at 4°C. The next day, the sections were immersed in double-distilled water for 10 min, followed by the addition of 20 μL of Ponceau S staining solution for 30 min. The sections were then rinsed with double-distilled water, treated with phosphomolybdic acid solution for 1–2 min, and stained with Aniline Blue solution for 2 min, followed by rinsing with double-distilled water. The sections were subsequently dehydrated and sealed with neutral resin.

Immunohistochemical staining

Paraffin sectioning, followed by citrate antigen retrieval. Apply the endogenous peroxidase blocker for 10 min. Block with 5% Bovine Serum Albumin (BSA) and let it sit for 30 min. Add primary antibodies, including CD68 (1:100, ARG10514, arigobio), 3-Nitrotyrosine (3-NT) (1:100, bs-8551R, bioss), and α-SMA (1:500, ARG66381, arigo), and incubate overnight at 4°C. The next day, after immersing the sections in PBS three times, add the reaction enhancer and incubate at room temperature for 20 min. Then add the goat anti-mouse/rabbit IgG polymer and incubate at room

temperature for 1 h. Use DAB chromogenic solution, followed by haematoxylin staining for 2 min. Differentiate with hydrochloric acid alcohol differentiation solution for 3 s. After dehydration, seal the sections with neutral resin.

Immunofluorescence staining

The paraffin sections were de-waxed and subjected to citrate antigen retrieval. After fixation with paraformaldehyde for 20 min, the sections were treated with 20 μL of polyethylene glycol octylphenol ether (Triton X-100) for 2 min. The sections were then blocked with 5% BSA for 30 min. Primary antibodies were added, including Collagen III (1:200, 22734-1-AP, Proteintech), GPX4 (1:200, A1933, Abclonal), γ-H2AX (1:150, ab81299, abcam), and 8-OHdG (1:200, GTX41980, GeneTex), and incubated overnight at 4°C. The next day, secondary antibodies were added, either Alexa Fluor™ Plus 488 (Invitrogen, A32731) or Alexa Fluor™ Plus 555 (Invitrogen, A32727), and incubated at room temperature in the dark for 1 h. The sections were then mounted.

Dihydroethidium (DHE) fluorescent probe staining

The heart tissue sections are de-waxed, soaked in PBS three times for 5 min each, stained with DHE (1:600, Sigma, D7008) in the dark at room temperature for 10 min, rinsed in ddH_2O three times for 5 min each, and then sealed with an anti-quenching mounting medium containing DAPI (Beyotime, P0131).

Extraction of primary atrial myocytes from rat hearts

Neonatal rat atrial myocytes (NRAMs) were isolated from the atria of 24-hour-old SD rats. After wiping the body with 75% alcohol, the neonatal rats were decapitated with scissors to euthanize them. Then, the hearts were taken out and placed into DMEM/F12 medium, during which the ventricular parts were removed. After all the atrial tissues were extracted, they were minced. The minced tissues were then digested with trypsin at 37°C. After complete digestion of the tissues, the liquid in the centrifuge tube was filtered through a sieve and centrifuged at 1000 rpm for 5 min. The supernatant was discarded, and DMEM/F12 was added. The mixture was thoroughly mixed and transferred to a large culture dish. After 2 h, the culture medium containing atrial myocytes was transferred to a centrifuge tube, centrifuged at 1000 rpm for 5 min, the supernatant was discarded, thoroughly mixed with the culture medium, and transferred to a new culture dish.

RNA isolation and quantitative real-time PCR

After treating the tissue samples or cells with Trizol reagent (Invitrogen, Cat. No. 15596026CN), chloroform was added to the mixture at a ratio of Trizol:chloroform = 5:1. The mixture was then incubated on ice for 10 min. Subsequently, the mixture was centrifuged at 12 000 rpm for 15 min at 4°C. An equal volume of isopropanol was added to the upper aqueous phase, and the mixture was incubated at −20°C for 1 h. The mixture was centrifuged again at 12 000 rpm for 15 min at 4°C. The supernatant was discarded, and pre-cooled 75% ethanol was added to the tube. The mixture was centrifuged once more, and the waste liquid was discarded. The RNA pellet was resuspended in an appropriate volume of DEPC-treated water, and 1 μL of the sample was used for quantification using a protein quantifier. cDNA synthesis was performed using a cDNA synthesis kit (YEASEN, Cat. No. 11141ES). RNA was reverse-transcribed into cDNA according to the reverse transcription protocol provided in the kit manual, and the synthesized cDNA was stored at −20°C. Real-time quantitative PCR was conducted using SYBR Green Master Mix (YEASEN, Cat. No. 11184ES). The primer sequences are listed in *Table 1*.

Western blot

After treating tissue samples or cells with a lysis buffer mixture (RIPA lysis buffer (Beyotime, P0013B): protease inhibitor (Beyotime, P1045-1): phosphatase inhibitor (Beyotime, P1045-2): PSMF (Beyotime, ST507) = 100:1:1:1), place them in a centrifuge at 12 000 rpm, centrifuge at 4°C for 15 min, and extract the supernatant protein for quantification. After SDS-PAGE electrophoresis, transfer to a PVDF membrane. Block with 5% skim milk at room temperature for 1 h. Incubate in primary antibody against GSTP1 (1:1000, A19061, Abclonal), GPX4 (1:1000, A1933, Abclonal), FTH (1:1000, A19544, Abclonal), SLC7A11 (1:1000, A13685, Abclonal), NOX4 (1:1000, 14347-1-AP, Proteintech), and β-actin (1:4000, T0022, Affinity Biosciences) at 4°C overnight. Wash the membrane with configured TBST solution (15 min/3 times), incubate in a secondary antibody solution prepared in a certain ratio at room temperature for 1 h. Wash the membrane with TBST (15 min/3 times). And protein bands were visualized using the Odyssey DLx Infrared Imaging System.

Determination of malonic dialdehyde (MDA) and GPX in serum and cells

According to the instructions of MDA (Solarbio, BC0025) and GPX (Solarbio, BC1195) assay kits, determine the MDA content and GPX activity in mouse serum of each group and cells, and calculate the MDA content and GPX activity of each group.

MitoSOX red, DCFH-DA, JC-1 staining

Mitochondrial ROS levels were measured using MitoSOX Red (Invitrogen, M36008) mitochondrial superoxide indicators. NRAMs were treated with 1 μM MitoSox Red at 37°C for 15 min. The levels of oxidizing free radicals and superoxide anions were measured with -dichlorodihydrofluorescein (DCFH-DA, Beyotime, S0033S). DCFH-DA (10 μM) was incubated at 37°C in the dark for 30 min. Observe with fluorescence microscope. Add the pre-prepared JC-1 (DOJINDO, MT09) working liquid. It was cultured at 37°C in 5% CO_2 incubator for 30–60 min. The supernatant was removed and the cells were washed with PBS twice. The cells were observed under fluorescence microscope after adding Imaging Buffer Solution.

Collection of atrial tissues from patients

A total of six patients admitted to the First Affiliated Hospital of Dalian Medical University from January 2021 to June 2022 were included in this study. The study included three male patients ($n = 3$) and three matched control subjects in terms of age and gender ($n = 3$). Atrial tissue samples (atrial appendage) were obtained from routine excision during cardiac surgery with cardiopulmonary bypass, while the control group had no history of atrial fibrillation and showed no significant abnormalities in physical examination (routine examination, clinical examination, laboratory reports, ultrasound reports). Exclusion criteria included diabetes, stroke, thyroid disease, blood system and kidney diseases, acute or chronic infectious diseases, cancer, etc. Atrial tissues were used for real-time quantitative PCR and protein immunoblotting (western blot) to determine mRNA and protein expression levels. The research protocol was approved by the Ethics Committee of the First Affiliated Hospital of Dalian Medical University (PJ-KS-KY-2021-229), and all patients signed informed consent forms. All procedures were in compliance with national policies and regulations.

Proteomics

Atrial tissues were obtained from mice after electrical stimulation. The mice were euthanized via cervical dislocation while under anaesthesia. Saline group and Ang II group were extracted and concentration of the supernatant was measured using BCA kit. After Trypsin Digestion, Peptides resulting from trypsin digestion were desalted using Strata X C18 (Phenomenex) and then lyophilized under vacuum. The peptides were dissolved in 0.5 M TEAB and labelled according to the TMT labelling kit instructions. The simplified procedure is as follows: after thawing, the labelling reagents were dissolved in acetonitrile and mixed with the peptides, followed by incubation at room temperature for 2 h. After labelling, the peptides were desalted, lyophilized under vacuum, and then fractionated using high-pH reverse-phase HPLC with an Agilent 300Extend C18 column (5 μm particle size, 4.6 mm inner diameter, 250 mm length). The gradient for peptide fractionation was 8–32% acetonitrile at pH 9, over a 60 min period to separate into 60 fractions, which were then combined into 18 fractions. The combined fractions were lyophilized under vacuum for subsequent analysis. Finally, liquid chromatography-mass spectrometry (LC-MS) analysis and database searching were performed (Beijing Jingjie Biotechnology Co., Ltd). Kyoto Encyclopedia of Genes and Genomes

Table 1 Primer sequences

Species	Gene	Forward primer (5′–3′)	Reverse primer (5′–3′)
Human	β-ACTIN	GAGAAAATCTGGCACCACACC	GGATAGCACAGCCTGGATAGCAA
Human	GSTP1	TTGGGCTCTATGGGAAGGAC	GGGAGATGTATTTGCAGCGGA
Human	GPX4	GAGATCAAAGAGTTCGCCGC	GGAGAGACGGTGTCCAAACT
Mouse	β-ACTIN	GTGACGTTGACATCCGTAAAGA	GCCGGACTCATCGTACTCC
Mouse	GSTP1	ATGCCACCATACACCATTGTC	GGGAGCTGCCCATACAGAC
Mouse	Collagen Ⅲ	CTGTAACATGGAAACTGGGGAAA	CCATAGCTGAACTGAAAACCACC
Mouse	ANP	ACCTGCTAGACCACCTGGAG	CCTTGGCTGTTATCTTCGGTACCG
Mouse	BNP	GAGGTCACTCCTATCCTCTGG	GCCATTTCCTCCGACTTTTCTC

(KEGG) pathway analysis was conducted to screen for differential metabolic pathways. Data were graphed using Xiantao (www.xiantao.love/).

Ferroptosis pathway PCR array

Atrial tissues were obtained from mice after electrical stimulation. The mice were euthanized via cervical dislocation while under anaesthesia. Saline group and Ang II group were extracted using the Trizol method. After treating tissue samples or cells with Trizol, add chloroform vigorously shake. After 10 min, 12 000 rpm, 4°C for 15 min, add isopropanol to the upper aqueous phase, mix by inversion, 12 000 rpm, 4°C for 15 min. Add precooled 75% ethanol to the tube, centrifuge again, and discard the waste liquid. Add DEPC and quantification. cDNA synthesis was performed using a cDNA synthesis kit. Real-time quantitative PCR was conducted using SYBR Green Master Mix (WcGene Biotech Shanghai China). Fluorescent quantitative PCR Array detection was performed according to the Ferroptosis PCR Array genes. Data were graphed using Xiantao (www.xiantao.love/).

AAV9 vector delivery

Adeno-associated virus serotype 9 (AAV9) expressing full-length GSTP1 cDNA ($1.9 * 10^{12}$ vg/mL) was generated by Hanbio (Shanghai, China), according to the manufacturer's protocol. The construction process of AAV9 virus includes the following steps: Enzyme digestion of the vector, acquisition of the target fragment, ligation of the target fragment with the vector, bacterial liquid PCR identification, sequencing, plasmid extraction, adenovirus-associated virus packaging, adenovirus-associated virus purification, quality detection of adenovirus-associated virus, and titre detection. AAV9 carrying the GSTP1 gene under the cTnT promoter (AAV9-cTnT-GSTP1) was injected intravenously via the tail vein in a single dose into the indicated mice. The control mice were injected with an equal volume of AAV9-control. After two weeks, we assayed its overexpression efficiency by qPCR.

Statistics

All statistical analyses were performed using GraphPad Prism 10.0 software, and experimental data were presented as mean ± standard deviation (mean ± SD). The Shapiro-Wilk test was used to evaluate the normality distribution in all cases. Statistical analyses were performed by parametric analysis: For comparison between two groups, *t*-tests were used to analyse statistical differences. For four-group data, one-way ANOVA analysis was used for statistical analysis. Nonparametric analyses were employed: Mann–Whitney *U* test for two groups or a Kruskal–Wallis test followed by Dunn's multiple comparison tests for three/four groups. A significance level of $*P < 0.05$, $**P < 0.01$, $***P < 0.001$, and $****P < 0.0001$ was considered statistically significant, n.s.: not significant.

Ethics

All animal experiments were conducted according to the standards of the Dalian Medical University Animal Experiment Management Committee (approval number: AEE21079). The studies involving human participants were reviewed and approved by the First Affiliated Hospital of Dalian Medical University (PJ-KS-KY-2021-229).

Consent to participate

The patients/participants provided their written informed consent to participate in this study.

Results

The ferroptosis pathway may be one of the important pathways for the occurrence of atrial fibrillation

We first constructed a mouse model of atrial fibrillation using Ang II. On the 20th day, the atrial size of the mice was measured by ultrasound. The results showed that, compared with the control group, the atria of Ang II-infused mice were significantly enlarged (*Figure 1A*). On the 21st day of infusion with Ang II or saline, atrial fibrillation was induced in mice by an automatic stimulator to detect the susceptibility to atrial fibrillation in each group. The study found that the incidence and duration of atrial fibrillation in Ang II-infused mice were significantly increased (*Figure 1B*). Fibrosis and oxidative stress in the atria of mice were detected by Masson staining and DHE staining. The results showed that, compared with the control group, the levels of fibrosis and oxidative stress were significantly increased in the atria of mice infused with Ang II for 3 weeks (*Figure 1C* and *D*). qPCR revealed that, compared with the control group, the expression levels of ANP, BNP, and Collagen III mRNA were significantly elevated in the atria of Ang II-infused mice (*Figure 1E* and *F*). This indicates that the mouse model of atrial fibrillation was successfully constructed. To clarify which pathway play important roles in mouse atrial fibrillation, we performed proteomic analysis on atrial tissues of the saline group and the Ang II group. The study found that, compared with the saline group, 574 proteins were up-regulated and 315 proteins were down-regulated in the Ang II group (*Figure 1G* and *H*). Based on KEGG pathway analysis, the ferroptosis signalling pathway was significantly different (*Figure 1I*). These results indicate that the ferroptosis pathway undergoes significant changes in mouse atrial fibrillation.

Ferroptosis inhibitor Fer-1 inhibits Ang II-induced atrial remodelling in mice

To further explore the impact of the ferroptosis pathway on atrial fibrillation in mice, we intraperitoneally injected ferroptosis inhibitor (Fer-1) one week before Ang II infusion for 4 weeks and measured the atrial size of the mice on the 20th day of Ang II infusion using ultrasound. The results showed that compared with the control group, the

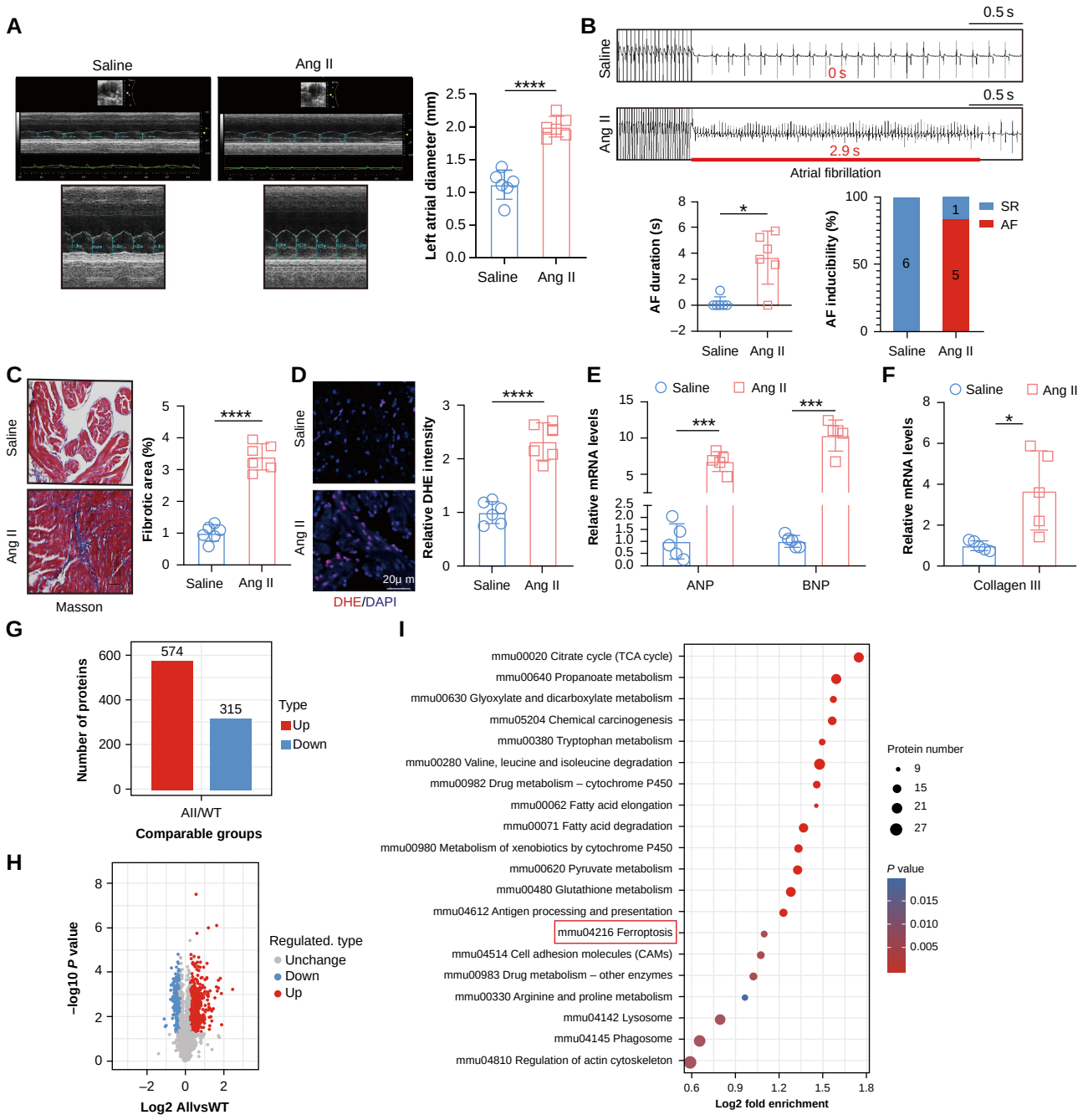

Figure 1 The ferroptosis pathway may be one of the important pathways for the occurrence of atrial fibrillation. (*A*) Representative echocardiographic images of left atrial dilation and quantitative analysis of left atrial dilation ($n = 6$); (*B*) representative atrial electrogram recordings, percentage of atrial fibrillation inducibility, and total atrial fibrillation duration ($n = 6$); (*C*) Masson's trichrome staining images and statistical graphs of mice from various groups ($n = 6$); (*D*) dihydroethidium (DHE) staining of mice from various groups ($n = 6$); (*E*) qPCR detection of ANP and BNP expression in mice from various groups, with statistical graphs attached ($n = 5$); (*F*) qPCR detection of Collagen III expression in mice from various groups, with statistical graphs attached ($n = 5$); (*G*) number of differentially expressed proteins between the saline group and the Ang II group; (*H*) Volcano plot displaying differentially expressed proteins, providing a visual representation of changes in protein expression; (*I*) KEGG pathway analysis revealing metabolic pathways enriched by differentially expressed proteins, offering clues to understanding biological processes. Statistical analysis was performed with two-tailed unpaired Student's *t*-test (*A*, *C*–*F*), Mann–Whitney *U* test (*B*). A significance level of $^{*}P < 0.05$, $^{***}P < 0.001$, and $^{****}P < 0.0001$ was considered statistically significant.

atria of Ang II-infused mice were significantly enlarged, whereas treatment with Fer-1 alleviated Ang II-induced atrial enlargement (*Figure* 2*A*). On the 21st day of Ang II or saline infusion, AF susceptibility was detected in each group of mice using an automatic stimulator. The study found that the incidence and duration of atrial fibrillation (AF) were significantly increased in Ang II-infused mice. Fer-1 treatment

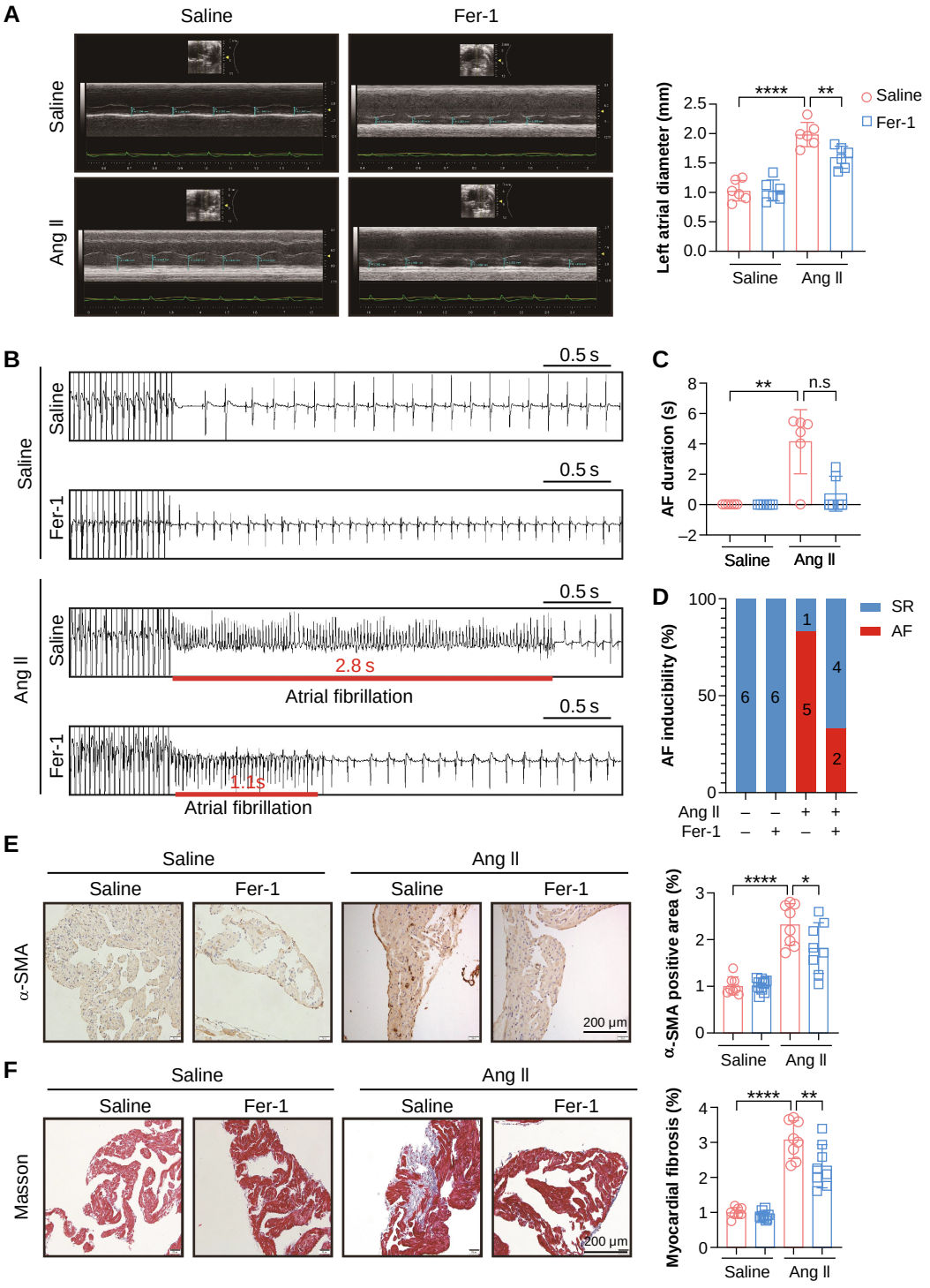

Figure 2 Ferroptosis inhibitor Fer-1 inhibits Ang II-induced atrial remodelling in mice. (*A*) Representative echocardiographic images of left atrial dilation and quantitative analysis of left atrial dilation ($n = 6$); (*B*) representative atrial electrogram recordings ($n = 6$); (*C*) total atrial fibrillation duration ($n = 6$); (*D*) percentage of atrial fibrillation inducibility ($n = 6$); (*E*) IHC staining of α-SMA images and statistical graphs of mice from various groups ($n = 8$); (*F*) Masson's trichrome staining images and statistical graphs of mice from various groups ($n = 8$). Statistical analysis was performed with one-way ANOVA (*A*, *E*, *F*), Kruskal–Wallis test (*C*). A significance level of $^{*}P < 0.05$, $^{**}P < 0.01$, and $^{****}P < 0.0001$ was considered statistically significant, ns: not significant.

reduced the incidence and duration of AF in Ang II-infused mice, although the differences did not reach statistical significance, a downward trend was observed. (*Figure 2B–D*). Atrial fibrosis in mice was detected using IHC (α-SMA) and Masson staining. The experimental results showed that compared with the control group, fibrosis increased after 3 weeks in the atrial tissue of Ang II-infused mice, whereas the degree of fibrosis induced by Ang II was reduced in Fer-1-treated mice (*Figure 2E* and *F*). Therefore, inhibiting the ferroptosis pathway can significantly intervene in Ang II-induced atrial fibrillation in mice.

GSTP1 changes in Ang II-induced atrial fibrillation found by ferroptosis microarray

In order to clarify which gene of ferroptosis pathway plays an important role in atrial fibrillation in mice, we performed ferroptosis PCR microarray analysis on the atrial tissues of normal saline group and Ang II group mice (*Figure 3A* and *Table 2*). The results showed that there were 11 genes with statistically significant differences, including seven up-regulated and four down-regulated genes (*Figure 3B*). Further verification by qPCR showed that the GSTP1 gene difference was the most significant (*Figure 3C*). Further, qPCR and western blot were used to detect the expression of ferroptosis pathway-related factors. The experimental results showed that compared with mice in saline group, the mRNA expression level of GSTP1 was significantly reduced in Ang-induced atrial fibrillation mice (*Figure 3D*). The levels of GSTP1, SLC7A11, GPX4, and FTH proteins were significantly reduced in Ang-induced mice, compared with those in the saline group (*Figure 3E*). These results indicated that the expression of GSTP1 was significantly decreased in Ang-induced atrial fibrillation mice, which was positively correlated with ferroptosis-related genes GSTP1 and GPX4. Next, we collected atrial tissue samples obtained from routine resection during surgery to explore the expression of ferroptosis-related genes in patients with atrial fibrillation. The mRNA expression of GSTP1 and GPX4 in the atria of patients with atrial fibrillation was significantly lower than that of the control group (*Figure 3F*). The protein levels of GSTP1 and GPX4 were detected by western blot. The experimental results showed that compared with the control group, the protein levels of GSTP1 and GPX4 in patients with atrial fibrillation were significantly reduced (*Figure 3G*). The above results show that ferroptosis-related genes and proteins in atrial fibrillation tissues will be significantly changed, and GSTP1 will be significantly decreased in atrial fibrillation tissues.

Overexpression of GSTP1 can improve Ang II-induced atrial enlargement and atrial fibrillation susceptibility

To further explore the effects of GSTP1 gene overexpression on Ang II-infused mice, the atrial size of mice was measured via ultrasound on the 20th day of Ang II or saline infusion. We first examined the infection efficiency of AAV9-cTNT-GSTP1. By detecting mRNA expression of GSTP1 in the hearts, livers, and lungs of mice, we found that GSTP1 was significantly overexpressed in the mouse hearts, while no statistically significant differences were observed in the livers and lungs (*Figure 4A*). Ultrasound results showed that compared with the control group, the atria of Ang II-infused mice were significantly enlarged, while GSTP1 gene overexpression could alleviate Ang II-induced atrial enlargement (*Figure 4B*). On the 21st day of Ang II or saline infusion, an automatic stimulator was used to induce atrial fibrillation in mice to detect the susceptibility of atrial fibrillation in each group. The study found that the incidence and duration of atrial fibrillation were significantly increased in Ang II-infused mice, while in Ang II mice with overexpressed GSTP1, the incidence and duration of atrial fibrillation were both reduced (*Figure 4C–E*). These results indicate that the overexpression of GSTP1 can attenuate Ang II-induced atrial enlargement and also reduce the incidence and shorten the duration of atrial fibrillation to some extent.

Overexpression of GSTP1 can improve Ang II-induced oxidative stress

Ferroptosis pathway is closely related to oxidative stress levels. To clarify the impact of GSTP1 gene overexpression on Ang II-induced oxidative stress, DHE fluorescence staining and 3-NT immunohistochemical staining were used to detect oxidative stress in mouse atria. Results showed that, compared with the control group, the fluorescence intensity and 3-NT expression levels in the atria of mice perfused with Ang II for 3 weeks were significantly increased. In contrast, in GSTP1 gene overexpression mice under Ang II perfusion, the atrial DHE fluorescence intensity and 3-NT expression levels were significantly reduced (*Figure 5A* and *B*). Meanwhile, by measuring the level of the oxidative stress factor NOX4, it was found that compared with the control group, the protein level of NOX4 in Ang II mice was significantly increased, while in GSTP1 gene overexpression mice, the NOX4 protein level was significantly reduced (*Figure 5C*). Additionally, by measuring the serum MDA content and GPX activity to assess the lipid peroxidation level in mice, it was found that the serum MDA level in Ang II-induced mice was significantly increased, and GPX activity was decreased. However, these changes were significantly alleviated in GSTP1 gene overexpression mice (*Figure 5D* and *E*).

Overexpression of GSTP1 gene can improve Ang II-induced inflammation and fibrosis

To further explore the effect of GSTP1 gene overexpression on Ang II-induced fibrosis, Masson staining was first used to detect atrial fibrosis in mice. The experimental results showed that compared with the control group, collagen deposition in atrial tissue increased after 3 weeks of Ang II infusion, whereas the degree of fibrosis induced by Ang II was reduced in mice with GSTP1 overexpression (*Figure 6A*). Further observation of the degree of fibrosis in atrial tissue through Collagen III (IF) and α-SMA (IHC) staining showed that, compared with the control group, the expression level of Collagen III and α-SMA in atrial tissue of Ang II-infused mice was elevated, while the degree of fibrosis was significantly alleviated in mice with GSTP1 overexpression (*Figure 6B* and *C*). To further explore the impact of GSTP1 overexpression on Ang II-induced inflammation, H&E staining results showed that infiltration of inflammatory cells in atrial tissue of Ang II-infused mice increased significantly, while this phenomenon was significantly reduced in mice with GSTP1 gene overexpression (*Figure 6D*). CD68 is a marker for changes in inflammatory factors and macrophages. Further observation of macrophage infiltration in atrial tissue through CD68 immunohistochemical staining showed that, compared with the control group, CD68 macrophage infiltration in atrial tissue of Ang II-infused mice increased, while the infiltration degree was significantly alleviated in mice with GSTP1 gene overexpression (*Figure 6E*).

Overexpression of GSTP1 can inhibit Ang II-induced oxidative stress, mitochondrial damage degree, and ferroptosis pathway in rat neonatal atrial myocytes

We experimentally demonstrated that GSTP1 can inhibit Ang II-induced atrial fibrillation in mice. Next, the protective effect of GSTP1 on Ang II-induced myocardial injury was explored *in vitro* experiments. First, the NRAMs were stimulated with different

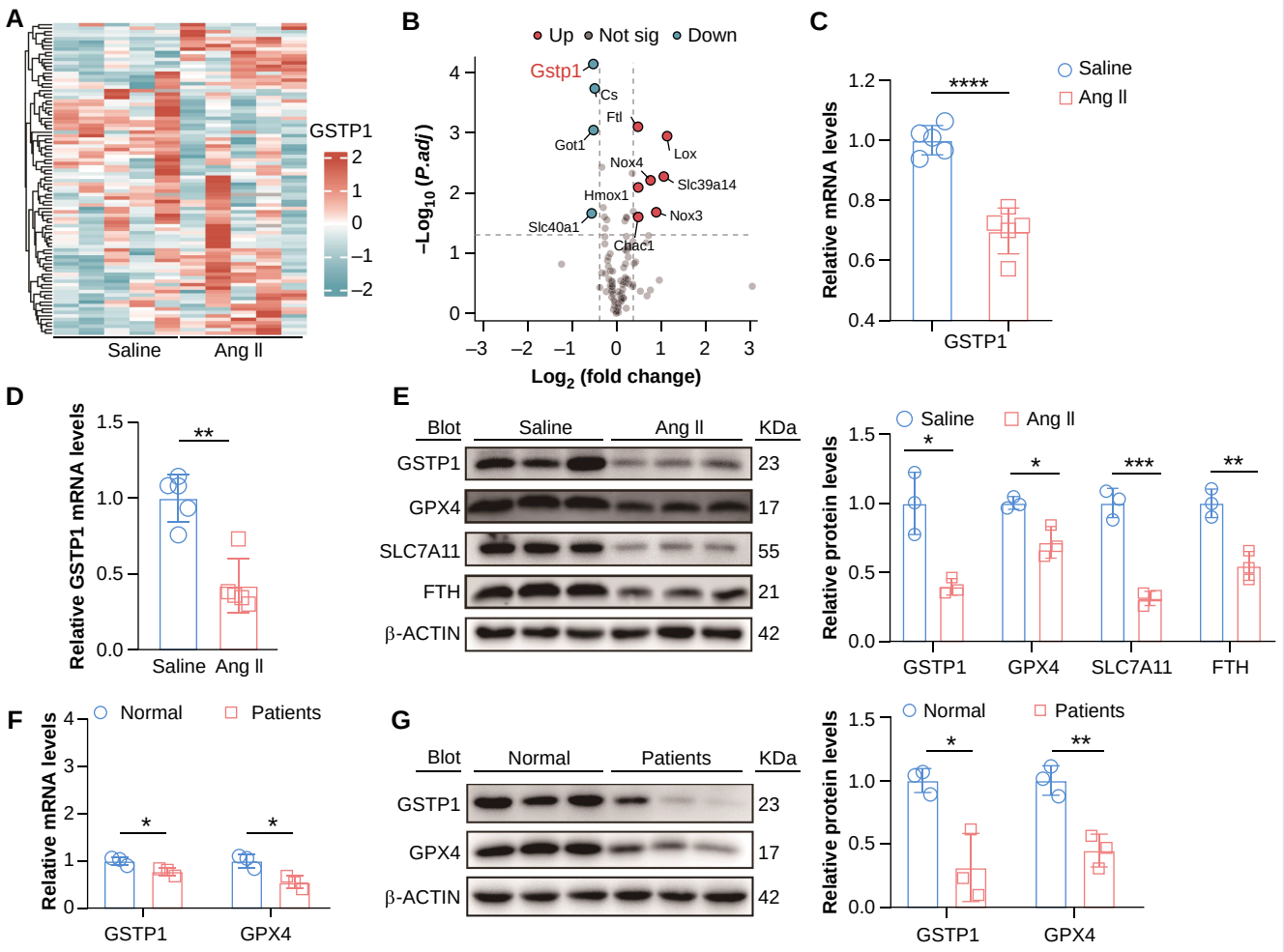

Figure 3 GSTP1 changes in Ang II-induced atrial fibrillation found by ferroptosis microarray. (*A*) Volcano plots were used to display the expression profiles of differentially expressed genes ($n = 5$); (*B*) the mRNA expression level of ferroptosis-related gene GSTP1 was analysed by qPCR and shown as Volcano plot ($n = 5$); (*C*) the expression of GSTP1 was detected by qPCR in the saline group and Ang II group ($n = 5$); (*D*) the expressions of GSTP1 and SLC40A1 were detected by qPCR in the saline group and Ang II group of mice ($n = 5$); (*E*) the expressions of GSTP1, GPX4, SLC7A11, FTH, and β-actin were detected by WB in the saline group and Ang II group of mice ($n = 3$); (*F*) the expressions of GSTP1, GPX4, and HO1 were detected by qPCR in patients ($n = 3$); (*G*) the expressions of GSTP1, GPX4, and SLC7A11 were detected by WB in patients ($n = 3$). Statistical analysis was performed with two-tailed unpaired Student's *t*-test (*C*, E-G), Mann–Whitney *U* test (*D*). A significance level of $^{*}P < 0.05$, $^{**}P < 0.01$, $^{***}P < 0.001$, and $^{****}P < 0.0001$ was considered statistically significant.

Table 2 List of ferroptosis genes

Mouse	1	2	3	4	5	6	7	8	9	10	11	12
A	Aco1	Arf6	Cars1	Dmt1	Gclc	Hamp	Hspb1	Ncoa4	Pcbp1	Sat2	Steap3	Vdac2
B	Acsl4	Atg5	Cdo1	Dpp4	Gclm	Hars	Ireb2	Nfe2l2	Pcbp2	Slc1a5	Stim1	Vdac3
C	Akr1b1	Atp5g3	Chac1	Elavl1	Gls2	Heph	Keap1	Nox1	Pparg	Slc39a14	Trf	Map1lc3b
D	Akr1b10	Bbc3	Cisd1	Emc2	Got1	Hfe	Kras	Nox3	Prdx6	Slc39a8	Tfr1	Panx2
E	Akr1c1	Becn1	Cisd2	Eprs	Gpx4	Hmox1	Lox	Nox4	Prnp	Slc3a2	Tfr2	Sat1
F	Aldh1a1	Braf	Cp	Fth1	Gss	Hmox2	Lpcat3	Nqo1	Ptges2	Slc40a1	Tp53	Sqstm1
G	Alox12	Brd4	Cs	Ftl	Gsta1	Hras	Map1lc3a	Nras	Rpl8	Slc7a11	Txnrd1	Usp7
H	Alox15	Ca9	Cybb	Ftmt	Gstp1	Hsf1	Actb	Gapdh	Hprt1	B2m	NTC	NTC

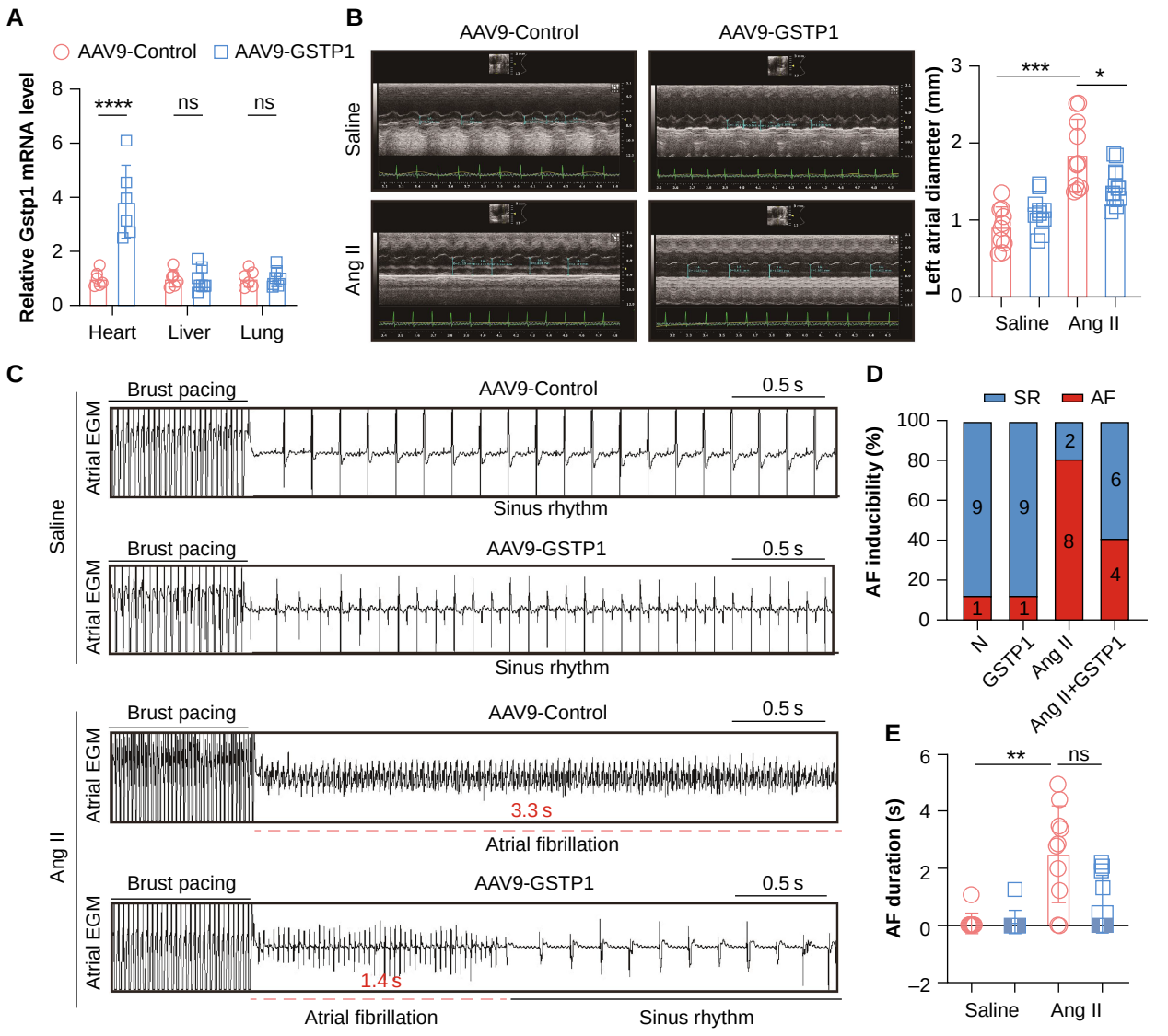

Figure 4 Overexpression of GSTP1 can improve Ang II-induced atrial enlargement and atrial fibrillation susceptibility. (*A*) The expression levels of GSTP1 mRNA in heart, liver and lung of each group of mice were detected by qPCR ($n = 6$). (*B*) Echocardiographic measurement LA dilation (left) and the quantification (right) in Ang II or saline-infused mouse ($n = 10$); (*C*) recordings of atrial fibrillation induced by an automatic stimulator ($n = 10$); (*D*) the percentage of atrial fibrillation induction in four groups of mice ($n = 10$); (*E*) the duration of atrial fibrillation in four groups of mice ($n = 10$). Statistical analysis was performed with one-way ANOVA (*A*, *B*), Kruskal–Wallis test (*E*). A significance level of $^{*}P < 0.05$, $^{**}P < 0.01$, and $^{***}P < 0.001$ was considered statistically significant; ns, not significant.

concentrations of Ang II, and it was proved by qPCR and WB experiments that the expression level of GSTP1 gradually decreased with the increase of Ang II concentration (*Figure 7A* and *B*). At the same time, we also verified that Ang II can inhibit the expression of GPX4 in NRAMs (*Figure 7C*). We constructed an overexpressing adenovirus of GSTP1 (Ad-GSTP1). It was demonstrated by qPCR that Ad-GSTP1 can significantly induce the expression of GSTP1 (*Figure 7D*). It was found by immunofluorescence (GPX4) that Ang II could significantly inhibit the expression of GPX4, while after overexpressing GSTP1, it increased the expression of GPX4 (*Figure 7E*). We performed DNA damage marker γ-H2ax. Similarly, it was found by immunofluorescence that Ang II could significantly induce the expression of γ-H2ax, but after overexpression of GSTP1, it inhibited the expression of γ-H2ax (*Figure 7F*). We used DCFH-DA to measure oxidative stress levels. The results showed that Ang II could significantly induce oxidative stress levels, while overexpressing GSTP1 inhibited oxidative stress levels (*Figure 7G*). We also made three markers (mitoSOX, JC-1 and 8-OHDG) for mitochondrial damage. The results showed that Ang II can significantly induce mitochondrial damage, while overexpressing GSTP1 inhibited mitochondrial damage (*Figure 7H–J*). We also did the ferroptosis pathway MDA and GPX activities, and the results showed that Ang II can significantly induce the expression of MDA and inhibit the activity of GPX, while the expression of MDA decreased significantly after overexpressing GSTP1, and the activity of GPX4 increased significantly (*Figure 7K*).

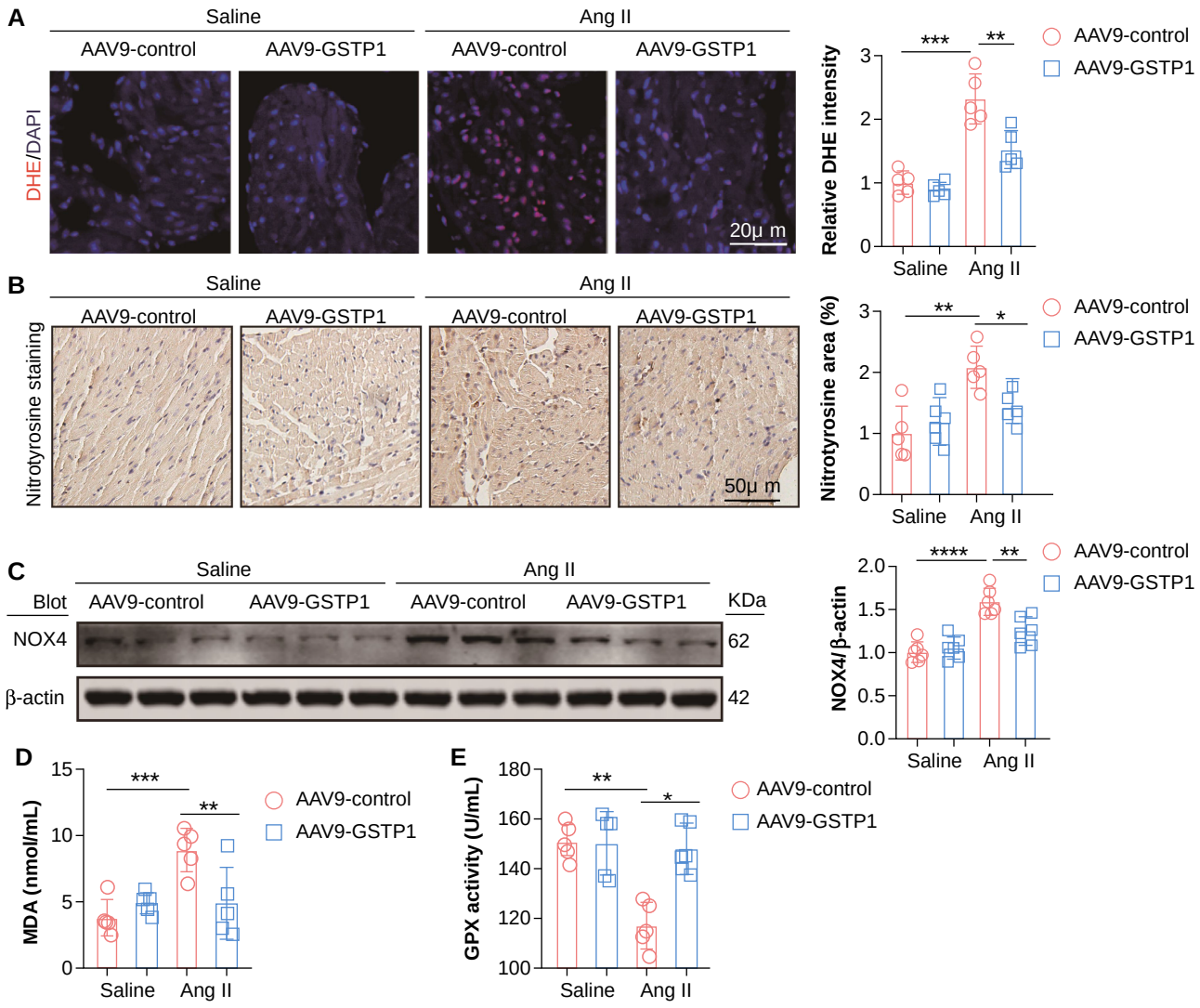

Figure 5 Overexpression of GSTP1 can improve Ang II-induced oxidative stress. (*A*) DHE fluorescence staining images (left) and their corresponding fluorescence intensity statistics (right) ($n = 5$); (*B*) 3-NT immunohistochemical staining images (left) and statistics of expression levels (right) ($n = 5$); (*C*) western blot analysis of NOX4 protein expression levels, a marker of oxidative stress, in mice from various groups ($n = 6$); (*D*) measurement of serum MDA content in mice from different groups ($n = 5$); (*E*) measurement of serum GPX activity in mice from various groups ($n = 5$). Statistical analysis was performed with one-way ANOVA (*A–E*). A significance level of $^{*}P < 0.05$, $^{**}P < 0.01$, $^{***}P < 0.001$, and $^{****}P < 0.0001$ was considered statistically significant.

Inhibition of GSTP1 can aggravate Ang II-induced oxidative stress, degree of mitochondrial damage, and ferroptosis pathway in NRAMs

We stimulated NRAMs with GSTP1 inhibitors Ezatiostat and Ang II, and found by immunofluorescence (GPX4) that Ang II could significantly inhibit GPX4 expression, while Ezatiostat further inhibited GPX4 expression (*Figure 8A*). We used DCFH-DA to measure oxidative stress levels. The results showed that Ang II could significantly induce oxidative stress levels, while Ezatiostat further induced oxidative stress levels (*Figure 8B*). It was also found by immunofluorescence that Ang II could significantly induce the expression of γ-H2ax, while Ezatiostat further promoted the expression of γ-H2ax (*Figure 8C*). We also performed mitochondrial damage marker (mitoSOX and 8-OHDG). The results showed that Ang II can significantly induce mitochondrial damage, while Ezatiostat further aggravates mitochondrial damage (*Figure 8D* and *E*). We also did the ferroptosis pathway MDA and GPX activities, and the results showed that Ang II can significantly induce the expression of MDA and inhibit the activity of GPX, while Ezatiostat further induces the expression of MDA and inhibits the activity of GPX (*Figure 8F*).

Discussion

Atrial fibrillation is the most common arrhythmia in clinical practice, increasing the risk of stroke, peripheral thromboembolism, and death in patients, thus imposing a heavy burden on social healthcare.[17] Ang II promotes the occurrence of atrial fibrillation by activating the Ang II

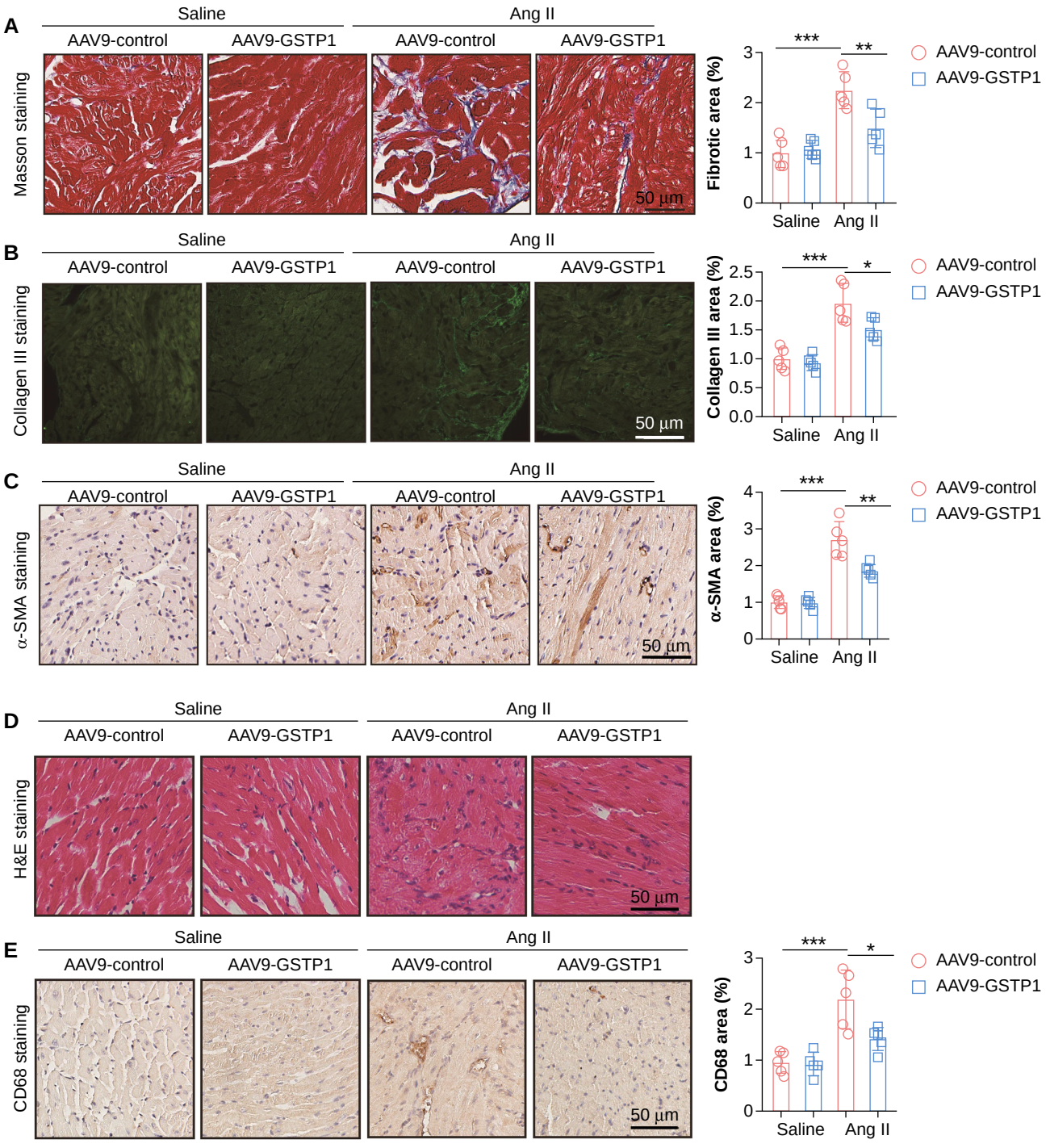

Figure 6 Overexpression of GSTP1 gene can improve Ang II-induced inflammation and fibrosis. (*A*) Masson staining images and their fibrosis degree statistics ($n = 5$); (*B*) Collagen III immunofluorescence staining images and their fluorescence intensity statistics ($n = 5$); (*C*) α-SMA immunohistochemical staining images and their positive degree statistics ($n = 5$); (*D*) H&E staining images ($n = 5$); (*E*) CD68 immunohistochemical staining images and their expression level statistics ($n = 5$). Statistical analysis was performed with one-way ANOVA (*A*–*E*). A significance level of $^{*}P < 0.05$, $^{**}P < 0.01$, and $^{***}P < 0.001$ was considered statistically significant.

type-1 receptor (AT1R), which triggers various complex signalling pathways, exacerbating cardiac inflammation, oxidative stress, and fibrosis.[18] The method of osmotic pump subcutaneous infusion of Angiotensin II (Ang II) is a reliable and repeatable technique that has been extensively validated in numerous studies.[19–22] The model exhibits structural and electrical remodelling in atria, and has been reported to be vulnerable to burst pacing-induced AF. As evidenced by previous studies, oxidized $Ca^{(2+)}$/calmodulin-dependent protein kinase II

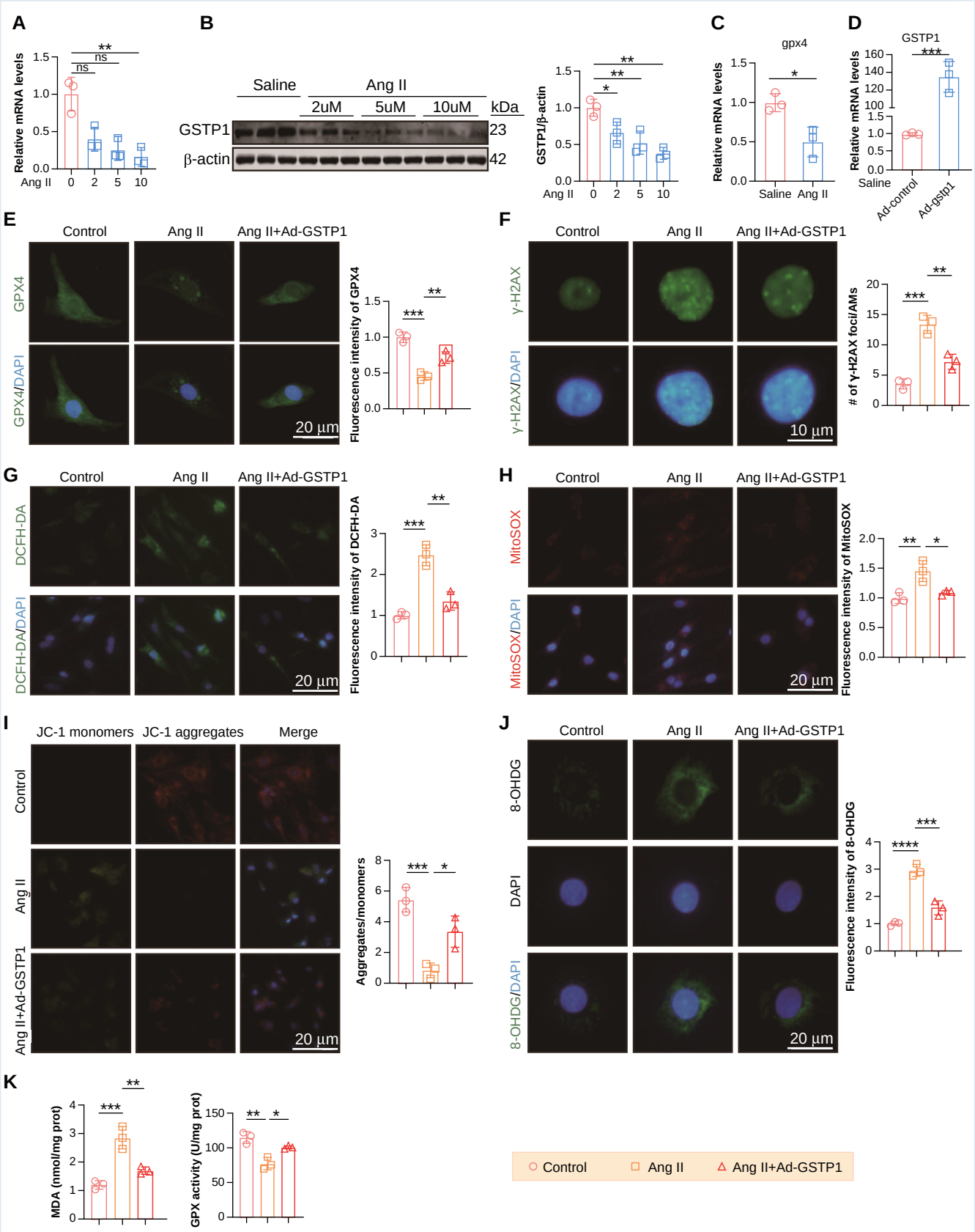

Figure 7 Overexpression of GSTP1 can inhibit Ang II-induced oxidative stress, mitochondrial damage degree, and ferroptosis pathway in rat neonatal atrial myocytes. (*A*) qPCR analysis of gstp1 expression ($n = 3$); (*B*) WB analysis of gstp1 expression ($n = 3$); (*C*) qPCR analysis of GPX4 expression

(continued)

(CaMKII) plays a pivotal role in triggering AF. This enzyme is highly sensitive to oxidative stress, which is often induced by Ang II infusion. The activation of CaMKII leads to the disruption of normal cardiac electrical activity, ultimately resulting in the development of AF.[23] In this study, an atrial fibrillation mouse model was constructed by subcutaneously implanting Alzet osmotic pumps to infuse Ang II. Proteomic analysis and KEGG pathway analysis of mouse atrial tissues were performed to screen for the role of ferroptosis signalling pathways in Ang II-induced myocardial injury in atrial fibrillation mice.

Atrial cardiomyopathy is a disease that affects atrial structure, contraction, or electrophysiological characteristics, and leads to atrial remodelling, electrical conduction dysfunction, and other related clinical manifestations.[24] Several studies have demonstrated that the relationship between AF and atrial myopathy is more complex. Atrial myopathy may exist without AF and can facilitate the development of AF.[25] Aging leads to advancing decline in the structure and function of the heart, and is a leading risk factor for atrial myopathy. Previous evidences have shown a close association between aging, atrial fibrillation, and stroke, which characterized by myocyte loss, reactive cellular hypertrophy, fibrosis, and autonomic nervous system dysregulation.[26] In some studies, male mice displayed AF susceptibility while females did not.[27] The Ang II mice we used were male and relatively young, so future research on elderly mice or female mice will be a new direction to explore.

Ferroptosis, a new research hotspot, has garnered significant attention for its role in heart diseases.[28] Ferroptosis is an important form of myocardial cell death involved in the development of various cardiovascular diseases, such as doxorubicin-induced cardiotoxicity, myocardial ischaemia-reperfusion, atrial fibrillation, and atherosclerosis.[29] We found that inhibiting the ferroptosis pathway can inhibit Ang II-induced atrial fibrillation by using ferroptosis inhibitors Fer-1. Studies have shown that the antioxidant factor NRF2 can inhibit lipid peroxidation and ferroptosis by regulating downstream target factors such as GSTP1, GPX4, SLC7A11, and HO-1.[30] This study found through ferroptosis PCR microarray analysis that GSTP1 RNA expression levels significantly decreased in Ang II-induced atrial fibrillation mice. Further modelling confirmed that RNA and protein levels of the GSTP1 gene were significantly reduced in Ang II-induced atrial fibrillation mice. Additionally, other key factors in the ferroptosis pathway, such as SLC7A11, GPX4, and FTH, were also significantly decreased. Furthermore, protein levels of GSTP1 in atrial tissues of atrial fibrillation patients were notably reduced. These results demonstrate that the ferroptosis pathway signalling factor GSTP1 is involved in the mechanism of myocardial injury in Ang II-induced atrial fibrillation mice.

GSTP1 is a member of the glutathione S-transferase (GST) family, which exerts detoxification effects by acting on glutathione.[31,32] GSTP1 plays a crucial role in regulating cellular oxidative stress and proliferation and is an important serum marker in heart failure patients.[33] GSTP1 inhibits cyclophosphamide-induced cardiotoxicity by detoxifying acrolein, and the cardiotoxicity induced by cyclophosphamide is exacerbated in GSTP1-deficient mice. Additionally, cardiac ischaemia increases acrolein in the heart, and GSTP1 deficiency makes ischaemia-reperfusion injury more sensitive, enlarging the infarct area after coronary artery occlusion.[34] This study constructed a GSTP1 overexpression mouse model via tail vein injection of adeno-associated virus to explore the role of GSTP1 in Ang II-induced atrial fibrillation mice. The results showed that compared with the Ang II group, the atrial fibrillation incidence in the Ang II + AAV9-GSTP1 group mice was reduced, and atrial enlargement was inhibited.

Ferroptosis, a novel form of regulated cell death, is characterized mainly by iron-dependent oxidative stress and increased lipid peroxidation.[35] MDA is a biomarker of oxidative stress in organisms. As a major degradation product of reactive oxygen species-induced lipid peroxidation, MDA is one of the main indicators of ferroptosis.[36,37] GPX activity can also serve as an important molecular marker for ferroptosis.[38] When GPX4 activity decreases, lipid peroxide products excessively accumulate, inducing ferroptosis.[39] This study detected serum MDA and GPX in each group of mice using respective assay kits, finding that compared with the control group, serum MDA levels significantly increased, and GPX activity significantly decreased in the Ang II group, while these changes were markedly alleviated in the Ang II + AAV9-GSTP1 group. These results provide evidence to some extent that GSTP1 overexpression inhibits ferroptosis in Ang II-induced atrial fibrillation mice.

The renin–angiotensin–aldosterone system can activate inflammatory and oxidative stress mediators, leading to endothelial dysfunction, thereby altering microcirculation and promoting subendocardial ischaemia, exacerbating myocardial fibrosis and cardiac sclerosis.[40] 3-NT, as a classic biomarker of oxidative stress, is closely related to cardiovascular diseases.[41] A case-control study showed that compared to the control group, the levels of 3-NT in cardiovascular disease patients were significantly increased, and the prevalence of cardiovascular disease also increased with elevated levels of 3-NT.[41] Immunohistochemical staining of 3-NT in mouse atrial tissue revealed that compared to the Ang II group, the levels of 3-NT in the Ang II + AAV9-GSTP1 group were significantly reduced. Additionally, NOX has the function of catalysing the production of reactive oxygen species by NADPH.[42] Among them, NOX4, as the main source of oxidative stress in heart failure, is abundantly expressed in the mitochondria of cardiomyocytes.[43] Subsequent analysis of NOX4 protein levels in mouse atrial tissue showed that compared to the Ang II group, the NOX4 protein levels in the Ang II + AAV9-GSTP1 group were significantly reduced. These results demonstrate that overexpression of GSTP1 can inhibit Ang II-induced oxidative stress to some extent.

Myocardial fibrosis and inflammation are the main pathological processes of myocardial remodelling.[44] As an important feature of atrial cardiomyopathy, fibrosis promotes the occurrence of atrial fibrillation.[45] Collagen III is produced by fibroblasts and other mesenchymal cells and is an important component of reticular fibres in the stromal tissues of the lungs, liver, heart, and blood vessels.[46] The degree of fibrosis in mouse atrial tissue was detected using Collagen III immunofluorescence staining and Masson staining. The results of this study found that compared to the Ang II group, the fibrosis level in the Ang II + AAV9-GSTP1 group was significantly reduced. It was found that a

Figure 7 Continued

($n = 3$); (*D*) qPCR assessment of Ad-gstp1 infection efficiency ($n = 3$); (*E*) immunofluorescence detection of GPX4 expression levels under ANG II and Ad-GSTP1 stimulation ($n = 3$); (*F*) immunofluorescence detection of H2aX expression levels under ANG II and Ad-GSTP1 stimulation ($n = 3$); (*G*) DCFH-DA assay to measure oxidative stress levels in cells from various groups under ANG II and Ad-GSTP1 stimulation ($n = 3$); (*H*) MitoSOX assay to assess mitochondrial damage in cells from different groups under ANG II and Ad-GSTP1 stimulation ($n = 3$); (*I*) JC-1 staining to evaluate mitochondrial damage in cells from various groups under ANG II and Ad-GSTP1 stimulation ($n = 3$); (*J*) immunofluorescence detection of 8-OHDG expression levels under ANG II and Ad-GSTP1 stimulation ($n = 3$); (*K*) measurement of serum MDA content and GPX activity in mice from different experimental groups ($n = 3$). Statistical analysis was performed with Kruskal–Wallis test (*A*) and one-way ANOVA (*B*–*K*). A significance level of $^{*}P < 0.05$, $^{**}P < 0.01$, $^{***}P < 0.001$, and $^{****}P < 0.0001$ was considered statistically significant.

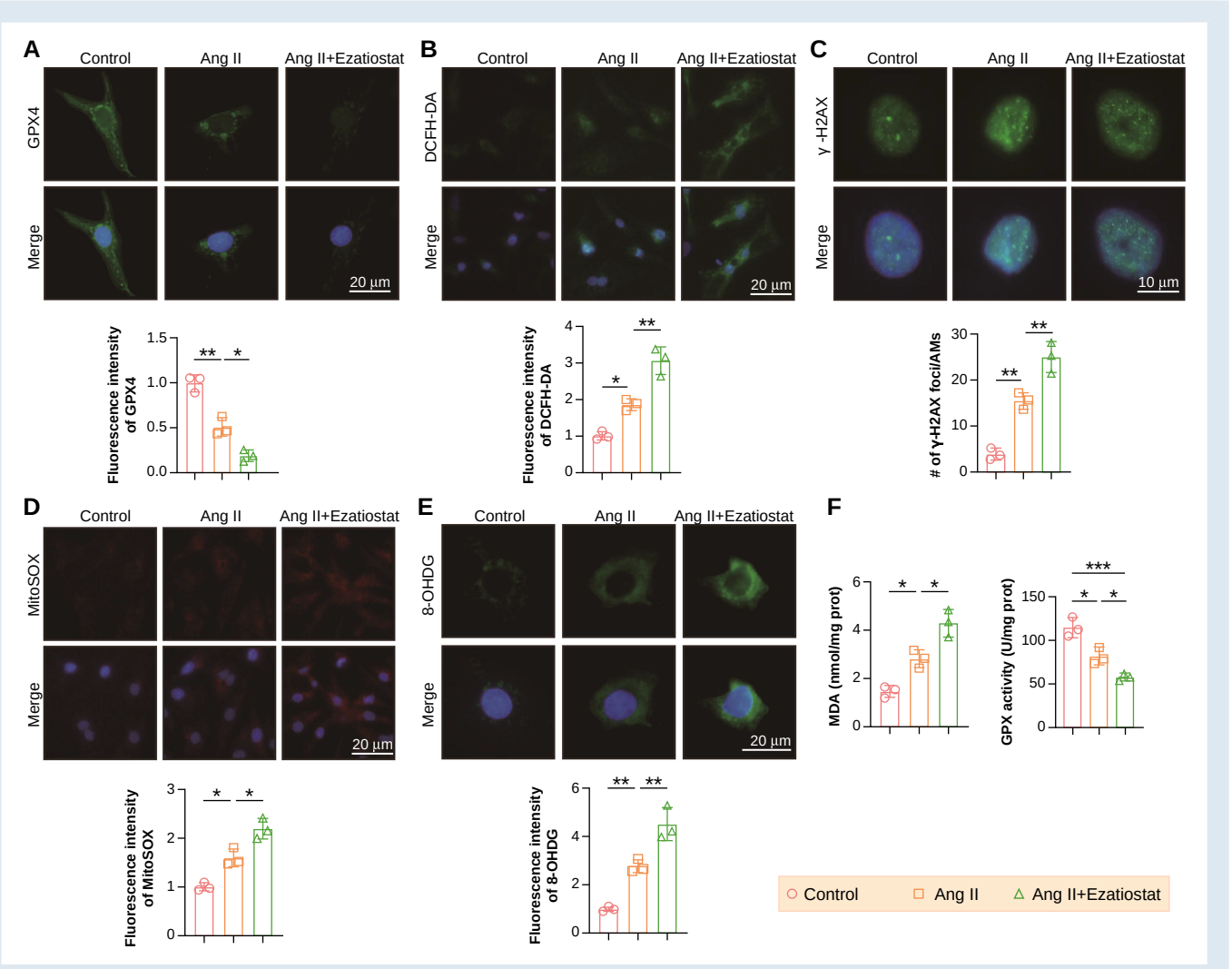

Figure 8 Inhibition of GSTP1 can aggravate Ang II-induced oxidative stress, degree of mitochondrial damage, and ferroptosis pathway in RNVMs. (*A*) Immunofluorescence detection of GPX4 expression levels under ANG II and Ad-GSTP1 stimulation ($n = 3$); (*B*) DCFH-DA assay to measure oxidative stress levels in cells from various groups under ANG II and Ad-GSTP1 stimulation ($n = 3$); (*C*) immunofluorescence detection of H2aX expression levels under ANG II and Ad-GSTP1 stimulation ($n = 3$)*n*; (*D*) MitoSOX assay to assess mitochondrial damage in cells from different groups under ANG II and Ad-GSTP1 stimulation ($n = 3$); (*E*) immunofluorescence detection of 8-OHDG expression levels under ANG II and Ad-GSTP1 stimulation ($n = 3$); (*F*) measurement of serum MDA content and GPX activity in mice from different experimental groups ($n = 3$). Statistical analysis was performed with one-way ANOVA (*A–F*). A significance level of $^{*}P < 0.05$, $^{**}P < 0.01$, and $^{***}P < 0.001$ was considered statistically significant.

single-dose injection of recombinant GSTP1 had a cardioprotective effect on rats after myocardial infarction and could inhibit the inflammatory response.[33] CD68 can identify macrophage populations, and CD68-positive cells are often observed in infiltrated cardiac tissue.[47] Furthermore, H&E staining and CD68 immunohistochemical staining were used to detect inflammation levels in mouse atrial tissue. This study showed that compared to the Ang II group alone, the degree of inflammatory cell and CD68 macrophage infiltration in the Ang II + AAV9-GSTP1 group was significantly reduced. These results to some extent demonstrate the protective role of GSTP1 in Ang II-induced atrial fibrillation.

GSTP1 can catalyse the reaction between glutathione and electrophilic agents, such as intracellular reactive oxygen species and hydroxyl radicals, inhibiting the oxidation of polyunsaturated fatty acids on the cell membrane and preventing ferroptosis.[32] GPX4 can act on glutathione to eliminate reactive oxygen species and inhibit lipid peroxidation, protecting cells from oxidative stress and serving as an important regulatory factor in ferroptosis.[48,49] Therefore, we observed changes in GPX4 levels by adding the GSTP1 inhibitor Ezatiostat and infecting neonatal rat primary atrial myocytes with adenovirus overexpressing GSTP1. Experimental results showed that compared to the control group, the protein levels of GPX4 in the Ezatiostat group were significantly decreased, while the protein levels of GPX4 were significantly increased after infection with adenovirus overexpressing GSTP1. This suggests that GSTP1 can regulate the activity of GPX4, inhibiting lipid peroxidation and ferroptosis (*Figure 9*).

In summary, we have found that the occurrence of atrial fibrillation (AF) is closely related to the ferroptosis metabolic pathway. GSTP1, as a key factor in the ferroptosis pathway, plays an important role in Angiotensin II (Ang II)-induced cardiomyocyte injury. Research has proved that GSTP1 can inhibit JNK signalling by interaction with the C terminus to form a GSTP1/JNK heterocomplex.[50] In non-stressed

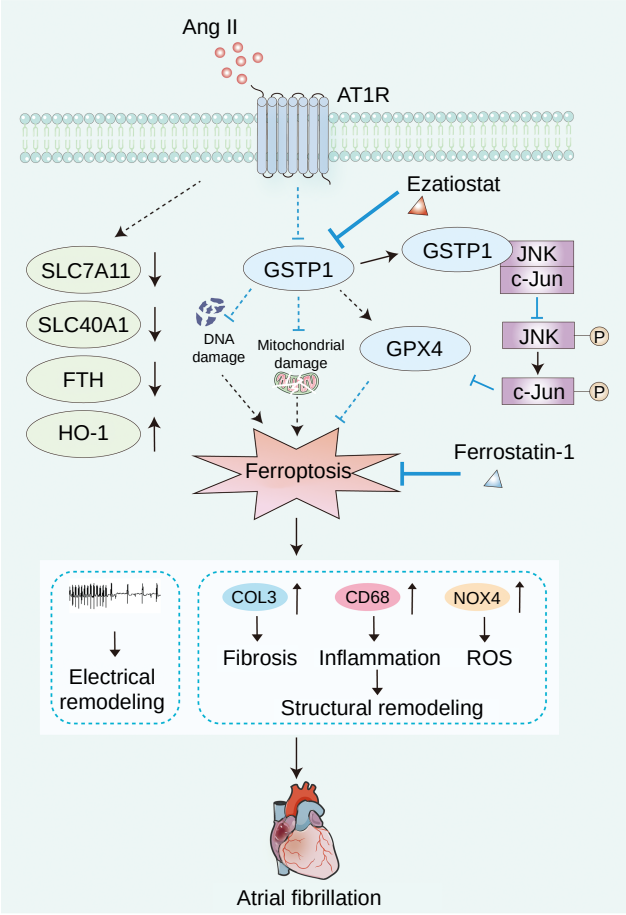

Figure 9 Schematic representation of the mechanism.

cells, GSTP1 can restrain the activation of JNK by binding to the C-terminal of JNK kinase, forming a GSTP1–JNK heterocomplex. Stimulus can trigger dissociation of the GSTP1–JNK heterocomplex resulted in the activation of JNK/c-Jun signalling pathway.[51] The activation of JNK is a pivotal factor leading to the accumulation of ROS, which in turn triggers the occurrence of ferroptosis. A study showed that Galangin alleviated Doxorubicin-induced cardiotoxicity by inhibiting ferroptosis through GSTP1/JNK pathway.[52] GSTP1 inhibits ferroptosis by GST and selenium-independent PH-GPx activities. Modulation of GSTP1 activity may present new opportunities for treatment development because GSTP1 catalyses the conjugation of GSH with 4-HNE and dramatically reduces subsequent lipid peroxidation.[53] Therefore, JNK or 4-HNE, as potential molecular targets, can be chosen for in-depth study. Besides, Biomarkers can be used for risk stratification and as treatment response predictors, which may approve in the early detection and adjustment of AF treatment. Both blood-derived molecular markers and ECG features have been used as biomarkers, such as the level of circulating galectin-3 and 12-lead ECGs.[54] The abnormal methylation of GSTP1 promoter, as a highly specific diagnostic marker for prostate cancer, is related to the development and prognosis of a series of tumour types.[55] This study may have a certain application prospect in predicting atrial fibrillation or recurrence of atrial fibrillation in the future. In our study, we observed a significant down-regulation of GSTP1 expression in Ang II-induced AF. Furthermore, by constructing a GSTP1 overexpression mouse model, we found that GSTP1 overexpression significantly reduced Ang II-induced oxidative stress, fibrosis, and inflammation levels, and decreased the occurrence of cardiomyocyte injury. Additionally, in atrial myocytes, we discovered that GSTP1 can inhibit ferroptosis by enhancing the activity of GPX4. Therefore, these results preliminarily demonstrate that GSTP1-mediated ferroptosis plays a crucial role in Ang II-induced AF models and may serve as a potential therapeutic target for the treatment of atrial fibrillation.

Supplementary material

Supplementary material is available at *Europace* online.

Authors' contributions

H.L.: Data curation, Investigation, Project administration, Visualization, Writing—original draft, Formal analysis. Z.F.: Data curation, Investigation, Project administration, Visualization, Writing—original draft. B.L.: Data curation, Investigation, Project administration, Visualization. J.B.: Data curation, Investigation, Project administration, Visualization. Q.-y.L.: Data curation, Investigation, Project administration, Visualization. X.Y.: Data curation, Investigation, Project administration, Visualization. N.Z.: Conception and design of research, Writing—review & editing, Supervision. X.Y.: Conception and design

of research, Writing—review & editing, Supervision. Y.X.: Conception and design of research, Writing—original draft, Formal analysis, Supervision.

Funding

This work was supported by the Natural Science Foundation of Liaoning Provincial (2024-MS-160), National Natural Science Foundation of China (82070380), the LiaoNing Revitalization Talents Program (XLYC2203195), National Key Research and Development Program of China (2022YFC2405002), the Dalian Science Fund for Distinguished Young Scholars (2022RJ13), DMU-1&DICP (UN202201), and Dalian Medical University Interdisciplinary Research Cooperation Project Team Funding (grant no. JCHZ2023012).

Conflict of interest: none declared.

Data availability

Data underlying this article will be shared upon reasonable request with the corresponding author.

References

1. Yamamoto C, Trayanova NA. Atrial fibrillation: insights from animal models, computational modeling, and clinical studies. *EBioMedicine* 2022;**85**:104310.
2. Cao W, Song S, Fang G, Li Y, Wang Y, Wang QS. Cadherin-11 deficiency attenuates Ang-II-induced atrial fibrosis and susceptibility to atrial fibrillation. *J Inflamm Res* 2021; **14**:2897–911.
3. Hong EY, Kim TY, Hong GU, Kang H, Lee JY, Park JY *et al.* Inhibitory effects of roseoside and icariside E4 isolated from a natural product mixture (No-ap) on the expression of angiotensin II receptor 1 and oxidative stress in angiotensin II-stimulated H9C2 cells. *Molecules* 2019;**24**:414.
4. Li H, Lin L, Xia YL, Xie Y, Yang X. Research progress on the role of ferroptosis in cardiovascular disease. *Front Cardiovasc Med* 2022;**9**:1077332.
5. Dodson M, Castro-Portuguez R, Zhang DD. Nrf2 plays a critical role in mitigating lipid peroxidation and ferroptosis. *Redox Biol* 2019;**23**:101107.
6. Zhang X, Yu Y, Lei H, Cai Y, Shen J, Zhu P *et al.* The Nrf-2/Ho-1 signaling axis: a ray of hope in cardiovascular diseases. *Cardiol Res Pract* 2020;**2020**:5695723.
7. Hu H, Chen Y, Jing L, Zhai C, Shen L. The link between ferroptosis and cardiovascular diseases: a novel target for treatment. *Front Cardiovasc Med* 2021;**8**:710963.
8. Fang X, Ardehali H, Min J, Wang F. The molecular and metabolic landscape of iron and ferroptosis in cardiovascular disease. *Nat Rev Cardiol* 2022;**20**:7–23.
9. Xu L, Fan Y, Wu L, Zhang C, Chu M, Wang Y *et al.* Exosomes from bone marrow mesenchymal stem cells with overexpressed Nrf2 inhibit cardiac fibrosis in rats with atrial fibrillation. *Cardiovasc Ther* 2022;**2022**:2687807.
10. Dai C, Kong B, Qin T, Xiao Z, Fang J, Gong Y *et al.* Inhibition of ferroptosis reduces susceptibility to frequent excessive alcohol consumption-induced atrial fibrillation. *Toxicology* 2022;**465**:153055.
11. Michalczyk K, Kapczuk P, Witczak G, Bosiacki M, Kurzawski M, Chlubek D *et al.* The associations between metalloestrogens, GSTP 1, and SLC11A2 polymorphism and the risk of endometrial cancer. *Nutrients* 2022;**14**:3079.
12. Simeunovic D, Odanovic N, Pljesa-Ercegovac M, Radic T, Radovanovic S, Coric V *et al.* Glutathione transferase p1 polymorphism might be a risk determinant in heart failure. *Dis Markers* 2019;**2019**:6984845.
13. Cui J, Li G, Yin J, Li L, Tan Y, Wei H *et al.* GSTP1 and cancer: expression, methylation, polymorphisms and signaling (review). *Int J Oncol* 2020;**56**:867–78.
14. Chen D, Liu J, Rui B, Gao M, Zhao N, Sun S *et al.* GSTpi protects against angiotensin II-induced proliferation and migration of vascular smooth muscle cells by preventing signal transducer and activator of transcription 3 activation. *Biochim Biophys Acta* 2014; **1843**:454–63.
15. Conklin DJ, Haberzettl P, Jagatheesan G, Baba S, Merchant ML, Prough RA *et al.* Glutathione S-transferase P protects against cyclophosphamide-induced cardiotoxicity in mice. *Toxicol Appl Pharmacol* 2015;**285**:136–48.
16. Zhu Y, Chen Y, Wang Y, Zhu Y, Wang H, Zuo M *et al.* Glutathione S-transferase-Pi 1 protects cells from irradiation-induced death by inhibiting ferroptosis in pancreatic cancer. *FASEB J* 2024;**38**:e70033.
17. Sagris M, Vardas EP, Theofilis P, Antonopoulos AS, Oikonomou E, Tousoulis D. Atrial fibrillation: pathogenesis, predisposing factors, and genetics. *Int J Mol Sci* 2021;**23**:6.
18. Zhang YL, Cao HJ, Han X, Teng F, Chen C, Yang J *et al.* Chemokine receptor CXCR-2 initiates atrial fibrillation by triggering monocyte mobilization in mice. *Hypertension* 2020;**76**:381–92.
19. Li D, Liu Y, Li C, Zhou Z, Gao K, Bao H *et al.* Spexin diminishes atrial fibrillation vulnerability by acting on galanin receptor 2. *Circulation* 2024;**150**:111–27.
20. Wang H, Liu M, Wang X, Shuai W, Fu H. Mfap4 deletion attenuates the progression of angiotensin II-induced atrial fibrosis and atrial fibrillation. *Europace* 2022;**24**:340–7.
21. Fakih W, Mroueh A, Gong DS, Kikuchi S, Pieper MP, Kindo M *et al.* Activated factor X stimulates atrial endothelial cells and tissues to promote remodelling responses through AT1R/ NADPH oxidases/SGLT1/2. *Cardiovasc Res* 2024;**120**:1138–54.
22. Wang Y, Wang J, Shi L, Chen X, Li D, Cui C *et al.* Cib2 is a novel endogenous repressor of atrial remodeling. *Circulation* 2023;**147**:1758–76.
23. Zhan G, Wang X, Wang X, Li J, Tang Y, Bi H *et al.* Dapagliflozin: a sodium-glucose cotransporter 2 inhibitor, attenuates angiotensin II-induced atrial fibrillation by regulating atrial electrical and structural remodeling. *Eur J Pharmacol* 2024;**978**: 176712.
24. Goette A, Kalman JM, Aguinaga L, Akar J, Cabrera JA, Chen SA *et al.* EHRA/HRS/APHRS/SOLAECE expert consensus on atrial cardiomyopathies: definition, characterization, and clinical implication. *Europace* 2016;**18**:1455–90.
25. Shen MJ, Arora R, Jalife J. Atrial myopathy. *JACC Basic Transl Sci* 2019;**4**:640–54.
26. Goette A, Corradi D, Dobrev D, Aguinaga L, Cabrera JA, Chugh SS *et al.* Atrial cardiomyopathy revisited-evolution of a concept: a clinical consensus statement of the European heart rhythm association (EHRA) of the ESC, the Heart Rhythm Society (HRS), the Asian Pacific Heart Rhythm Society (APHRS), and the Latin American Heart Rhythm Society (LAHRS). *Europace* 2024;**26**:euae204.
27. Ripplinger CM, Glukhov AV, Kay MW, Boukens BJ, Chiamvimonvat N, Delisle BP *et al.* Guidelines for assessment of cardiac electrophysiology and arrhythmias in small animals. *Am J Physiol Heart Circ Physiol* 2022;**323**:H1137–66.
28. Yu Y, Yan Y, Niu F, Wang Y, Chen X, Su G *et al.* Ferroptosis: a cell death connecting oxidative stress, inflammation and cardiovascular diseases. *Cell Death Discov* 2021;**7**:193.
29. Del RD, Amgalan D, Linkermann A, Liu Q, Kitsis RN. Fundamental mechanisms of regulated cell death and implications for heart disease. *Physiol Rev* 2019;**99**:1765–817.
30. Xie X, Shen TT, Bi HL, Su ZL, Liao ZQ, Zhang Y *et al.* Melatonin inhibits angiotensin II-induced atrial fibrillation through preventing degradation of Ang II type I receptor-associated protein (ATRAP). *Biochem Pharmacol* 2022;**202**:115146.
31. Lei X, Du L, Yu W, Wang Y, Ma N, Qu B. GSTP1 as a novel target in radiation induced lung injury. *J Transl Med* 2021;**19**:297.
32. Tan X, Huang X, Niu B, Guo X, Lei X, Qu B. Targeting GSTP1-dependent ferroptosis in lung cancer radiotherapy: existing evidence and future directions. *Front Mol Biosci* 2022; **9**:1102158.
33. Andrukhova O, Salama M, Krssak M, Wiedemann D, El-Housseiny L, Hacker M *et al.* Single-dose GSTP1 prevents infarction-induced heart failure. *J Card Fail* 2014;**20**: 135–45.
34. Conklin DJ, Guo Y, Jagatheesan G, Kilfoil PJ, Haberzettl P, Hill BG *et al.* Genetic deficiency of glutathione S-transferase P increases myocardial sensitivity to ischemia-reperfusion injury. *Circ Res* 2015;**117**:437–49.
35. Yao Q, Sun R, Bao S, Chen R, Kou L. Bilirubin protects transplanted islets by targeting ferroptosis. *Front Pharmacol* 2020;**11**:907.
36. Tungmunnithum D, Abid M, Elamrani A, Drouet S, Addi M, Hano C. Almond skin extracts and chlorogenic acid delay chronological aging and enhanced oxidative stress response in yeast. *Life (Basel)* 2020;**10**:80.
37. Yao F, Cui X, Zhang Y, Bei Z, Wang H, Zhao D *et al.* Iron regulatory protein 1 promotes ferroptosis by sustaining cellular iron homeostasis in melanoma. *Oncol Lett* 2021;**22**:657.
38. Chu J, Liu CX, Song R, Li QL. Ferrostatin-1 protects HT-22 cells from oxidative toxicity. *Neural Regen Res* 2020;**15**:528–36.
39. Chen Z, Yan Y, Qi C, Liu J, Li L, Wang J. The role of ferroptosis in cardiovascular disease and its therapeutic significance. *Front Cardiovasc Med* 2021;**8**:733229.
40. Goidescu CM, Chiorescu RM, Diana ML, Mocan M, Stoia MA, Anton FP *et al.* ACE2 and apelin-13: biomarkers with a prognostic value in congestive heart failure. *Dis Markers* 2021;**2021**:5569410.
41. Daiber A, Hahad O, Andreadou I, Steven S, Daub S, Munzel T. Redox-related biomarkers in human cardiovascular disease—classical footprints and beyond. *Redox Biol* 2021; **42**:101875.
42. Liu Y, Huang Y, Xu C, An P, Luo Y, Jiao L *et al.* Mitochondrial dysfunction and therapeutic perspectives in cardiovascular diseases. *Int J Mol Sci* 2022;**23**:16053.
43. Kuroda J, Ago T, Matsushima S, Zhai P, Schneider MD, Sadoshima J. NADPH oxidase 4 (Nox4) is a major source of oxidative stress in the failing heart. *Proc Natl Acad Sci U S A* 2010;**107**:15565–70.
44. Wang LP, Han RM, Wu B, Luo MY, Deng YH, Wang W *et al.* Mst1 silencing alleviates hypertensive myocardial injury associated with the augmentation of microvascular endothelial cell autophagy. *Int J Mol Med* 2022;**50**:146.
45. Mccauley MD, Iacobellis G, Li N, Nattel S, Goldberger JJ. Targeting the substrate for atrial fibrillation: JACC review topic of the week. *J Am Coll Cardiol* 2024; **83**:2015–27.
46. Nikolov A, Popovski N. Extracellular matrix in heart disease: focus on circulating collagen type I and III derived peptides as biomarkers of myocardial fibrosis and their potential in the prognosis of heart failure: a concise review. *Metabolites* 2022;**12**:297.
47. Pei ZW, Guo Y, Zhu HL, Dong M, Zhang Q, Wang F. Thymoquinone protects against hyperlipidemia-induced cardiac damage in low-density lipoprotein receptor-deficient

(LDL-$^{R-/-}$) mice via its anti-inflammatory and antipyroptotic effects. *Biomed Res Int* 2020;**2020**:4878704.
48. Lei G, Zhang Y, Koppula P, Liu X, Zhang J, Lin SH *et al.* The role of ferroptosis in ionizing radiation-induced cell death and tumor suppression. *Cell Res* 2020;**30**:146–62.
49. Wang H, Liu C, Zhao Y, Gao G. Mitochondria regulation in ferroptosis. *Eur J Cell Biol* 2020;**99**:151058.
50. Wang T, Arifoglu P, Ronai Z, Tew KD. Glutathione S-transferase P1-1 (GSTP1-1) inhibits c-Jun N-terminal kinase (JNK1) signaling through interaction with the C terminus. *J Biol Chem* 2001;**276**:20999–1003.
51. Llavanera M, Mateo-Otero Y, Delgado-Bermudez A, Recuero S, Olives S, Barranco I *et al.* Deactivation of the JNK pathway by GSTP1 is essential to maintain sperm functionality. *Front Cell Dev Biol* 2021;**9**:627140.
52. Shu G, Chen K, Li J, Liu B, Chen X, Wang J *et al.* Galangin alleviated doxorubicin-induced cardiotoxicity by inhibiting ferroptosis through GSTP1/JNK pathway. *Phytomedicine* 2024;**134**:155989.
53. Zhang W, Dai J, Hou G, Liu H, Zheng S, Wang X *et al.* SMURF2 predisposes cancer cell toward ferroptosis in gpx4-independent manners by promoting GSTP1 degradation. *Mol Cell* 2023;**83**:4352–4369.e8.
54. Remme CA, Heijman J, Gomez AM, Zaza A, Odening KE. 25 years of basic and translational science in *EP Europace*: novel insights into arrhythmia mechanisms and therapeutic strategies. *Europace* 2023;**25**:euad210.
55. Pidsley R, Lam D, Qu W, Stricker P, Kench JG, Horvath LG *et al.* Investigating the prognostic utility of GSTP1 promoter methylation in prostate cancer. *BJUI Compass* 2024;**5**:1299–306.